CHEMISTRY
A EUROPEAN JOURNAL

DOI: 10.1002/chem.200903046

Ligand-to-Ligand Charge-Transfer Transitions of Platinum(II) Complexes with Arylacetylide Ligands with Different Chain Lengths: Spectroscopic Characterization, Effect of Molecular Conformations, and Density Functional Theory Calculations

Glenna So Ming Tong, Yuen-Chi Law, Steven C. F. Kui, Nianyong Zhu, King Hong Leung, David Lee Phillips, and Chi-Ming Che*[a]

Abstract: The complexes $[Pt(tBu_3tpy)\{C{\equiv}C(C_6H_4C{\equiv}C)_{n-1}R\}]^+$ ($n=1$: R = alkyl and aryl (Ar); $n=1$–3: R = phenyl (Ph) or Ph-$N(CH_3)_2$-4; $n=1$ and 2, R = Ph-NH_2-4; tBu_3tpy = 4,4',4''-tri-*tert*-butyl-2,2':6',2''-terpyridine) and $[Pt(Cl_3tpy)(C{\equiv}CR)]^+$ (R = *tert*-butyl (*t*Bu), Ph, 9,9'-dibutylfluorene, 9,9'-dibutyl-7-dimethyl-amine-fluorene; Cl_3tpy = 4,4',4''-trichloro-2,2':6',2''-terpyridine) were prepared. The effects of substituent(s) on the terpyridine (tpy) and acetylide ligands and chain length of arylacetylide ligands on the absorption and emission spectra were examined. Resonance Raman (RR) spectra of $[Pt(tBu_3tpy)(C{\equiv}CR)]^+$ (R = *n*-butyl, Ph, and C_6H_4-OCH_3-4) obtained in acetonitrile at 298 K reveal that the structural distortion of the C≡C bond in the electronic excited state obtained by 502.9 nm excitation is substantially larger than that obtained by 416 nm excitation. Density functional theory (DFT) and time-dependent DFT (TDDFT) calculations on $[Pt(H_3tpy)(C{\equiv}CR)]^+$ (R = *n*-propyl (*n*Pr), 2-pyridyl (Py)), $[Pt(H_3tpy)\{C{\equiv}C(C_6H_4C{\equiv}C)_{n-1}Ph\}]^+$ ($n=1$–3), and $[Pt(H_3tpy)\{C{\equiv}C(C_6H_4C{\equiv}C)_{n-1}C_6H_4$-$N(CH_3)_2-4\}]^+$/$+H^+$ ($n=1$–3; H_3tpy = nonsubstituted terpyridine) at two different conformations were performed, namely, with the phenyl rings of the arylacetylide ligands coplanar ("cop") with and perpendicular ("per") to the H_3tpy ligand. Combining the experimental data and calculated results, the two lowest energy absorption peak maxima, λ_1 and λ_2, of $[Pt(Y_3tpy)(C{\equiv}CR)]^+$ (Y = *t*Bu or Cl, R = aryl) are attributed to $^1[\pi(C{\equiv}CR){\rightarrow}\pi^*(Y_3tpy)]$ in the "cop" conformation and mixed $^1[d_\pi(Pt){\rightarrow}\pi^*(Y_3tpy)]/^1[\pi(C{\equiv}CR){\rightarrow}\pi^*(Y_3tpy)]$ transitions in the "per" conformation. The lowest energy absorption peak λ_1 for $[Pt(tBu_3tpy)\{C{\equiv}C(C_6H_4C{\equiv}C)_{n-1}C_6H_4$-H-4$\}]^+$ ($n=1$–3) shows a redshift with increasing chain length. However, for $[Pt(tBu_3tpy)\{C{\equiv}C(C6H4C{\equiv}C)_{n-1}C_6H_4$-$N(CH_3)_2-4\}]^+$ ($n=1$–3), λ_1 shows a blueshift with increasing chain length *n*, but shows a redshift after the addition of acid. The emissions of $[Pt(Y_3tpy)(C{\equiv}CR)]^+$ (Y = *t*Bu or Cl) at 524–642 nm measured in dichloromethane at 298 K are assigned to the $^3[\pi(C{\equiv}CAr){\rightarrow}\pi^*(Y_3tpy)]$ excited states and mixed $^3[d_\pi(Pt){\rightarrow}\pi^*(Y_3tpy)]/^3[\pi(C{\equiv}C){\rightarrow}\pi^*(Y_3tpy)]$ excited states for R = aryl and alkyl groups, respectively. $[Pt(tBu_3tpy)\{C{\equiv}C(C_6H_4C{\equiv}C)_{n-1}C_6H_4$-$N(CH_3)_2-4\}]^+$ ($n=1$ and 2) are nonemissive, and this is attributed to the small energy gap between the singlet ground state (S_0) and the lowest triplet excited state (T_1).

Keywords: density functional calculations · ligand effects · phosphorescence · photophysics · platinum · UV/Vis spectroscopy

Introduction

Studies on platinum(II) complexes containing acetylide ligands have received considerable interests in recent years.[1] In this area, a prototype is $[Pt(tpy)(C{\equiv}CR)]^+$ (tpy = 2,2':6',2''-terpyridine, R = aryl, alkyl) ,which has demonstrated interesting photophysical[1d,h] and nonlinear optical properties.[1a,i,2] Attachment of Pt^{II} to acetylide ligand(s) has a number of advantages: 1) the large spin-orbit coupling constant of Pt^{II} increases the rate of singlet–triplet intersys-

[a] Dr. G. S. M. Tong, Dr. Y.-C. Law, Dr. S. C. F. Kui, Dr. N. Zhu, Dr. K. H. Leung, Prof. D. L. Phillips, Prof. C.-M. Che
Department of Chemistry
Institute of Molecular Functional Materials
and HKU-CAS Joint Laboratory on New Materials
The University of Hong Kong, Pokfulam, Hong Kong SAR (China)
Fax: (+852) 22857-1586
E-mail: cmche@hku.hk

Supporting information for this article is available on the WWW under http://dx.doi.org/10.1002/chem.200903046.

tem crossing and phosphorescence efficiency; 2) the strong field acetylide ligand raises the energy of the d–d deactivation state; and 3) the p_π-orbitals of acetylide ligand mix with d_π(Pt) orbitals through π-conjugation, which facilitates charge migration and energy transfer.

Over the past several years, the spectroscopic properties of $[Pt(tpy)(C{\equiv}CR)]^+$ and related systems have been studied by various groups.[1–4] It has been shown that variation of the R substituent results in remarkable changes in the spectroscopic properties. For instance, the electronic excited states and photophysical properties, including emission energy, lifetime, and quantum yield, can be varied by the *para*-substituent of aryl acetylide ligands and are affected by external stimuli, such as acids[1a,b,4] and metal ions.[1a,4] Several assignments have been proposed for the lowest energy absorption bands of $[Pt(tpy)(C{\equiv}CR)]^+$ (R = aryl) at $\lambda_{max}>$ 400 nm including $^1[d_\pi(Pt){\rightarrow}\pi^*(tpy)]$ metal-to-ligand charge-transfer (^{1}MLCT),[1a,d] $^1[\pi(C{\equiv}CAr){\rightarrow}\pi^*(tpy)]$ ligand-to-ligand charge-transfer (^{1}LLCT),[1a,4] and an admixture of ^{1}MLCT and ^{1}LLCT transitions.[1a,g,2a] In early reports, the emission of $[Pt(tpy)(C{\equiv}CAr)]^+$ was assigned to the $^3[d_\pi(Pt){\rightarrow}\pi^*(tpy)]$ (^{3}MLCT) excited state. The $^3[\pi(C{\equiv}CAr){\rightarrow}\pi^*(tpy)]$ (^{3}LLCT) excited state is usually suggested to account for quenching of ^{3}MLCT emission.[1a,2a,4] Recent computational studies revealed that the lowest energy absorption and triplet emission of the Pt^{II} complexes containing aryl acetylide ligands with electron-donating amine substituents are solely derived from the $\pi(C{\equiv}CAr){\rightarrow}\pi^*(tpy)$ (LLCT) transition.[1g]

In the literature, there are a number of studies on the effect of aryl acetylide chain length on the spectroscopic and photophysical properties of metal aryl acetylide complexes, including $[Ru(tpy)(bpy)\{C{\equiv}C(C_6H_4C{\equiv}C)_{n-1}Ph\}]^+$ (n = 1–3; bpy = 2,2'-bipyridine, Ph = phenyl),[5] $[Au(Cy_3P)\{C{\equiv}C(C_6H_4C{\equiv}C)_{n-1}Ph\}]^+$ (n = 1–4; PCy_3 = tricyclohexylphosphine),[6] *trans*-$[Pt\{C{\equiv}C(C_6H_4C{\equiv}C)_{n-1}Ph\}_2]$ (n = 1–3),[7] and *trans*-$[Ru(dmpe)_2\{C{\equiv}C(C_6H_4C{\equiv}C)_{n-1}C_6H_4\text{-}X\text{-}4\}_2]$ (n = 1–3, X = H or $N(CH_3)_2$; dmpe = 1,5,9,13-tetramethyl-1,5,9,13-tetraazacyclohexadecane).[8] In these reported examples, the electronic transitions are MLCT $d_\pi(M){\rightarrow}\pi^*(C{\equiv}C(C_6H_4C{\equiv}C)_{n-1}Ph)$ and/or intraligand (IL) $\pi{\rightarrow}\pi^*(C{\equiv}C(C_6H_4C{\equiv}C)_{n-1}Ph)$ in nature. However, systematic studies on the effect of aryl acetylide chain length upon ligand-to-ligand charge-transfer (LLCT) transitions of transition-metal complexes are lacking. Since the terpyridine ligand has low-lying π* orbitals, $[Pt(tpy)\{C{\equiv}C(C_6H_4C{\equiv}C)_{n-1}C_6H_4\text{-}X\text{-}4\}]^+$ (n = 1–3, X = H or $N(CH_3)_2$; n = 1–2, X = NH_2) is a unique class of complexes for examining the effect of aryl acetylide chain length on LLCT transitions.

The aim of the present study is to elucidate the electronic transitions of platinum(II) acetylide complexes supported by the tBu$_3$tpy and Cl_3tpy ligands (tBu$_3$tpy = 4,4',4''-tri-*tert*-butyl-2,2':6',2''-terpyridine and Cl_3tpy = 4,4',4''-trichloro-2,2':6',2''-terpyridine). A group of alkyl acetylide ligands and aryl acetylide ligands with varied chain lengths were examined. The nature of the electronic transitions at $\lambda>$ 380 nm and the corresponding excited states were examined by combining both the data obtained by using UV/Vis absorption and resonance Raman (RR) spectroscopy and the results of quantum chemical calculations. At $\lambda>380$ nm, $[Pt(Y_3tpy)(C{\equiv}CR)]^+$ (Y = *tert*-butyl (tBu) or Cl, R = aryl) complexes show two partially overlapping absorption bands of different electronic origins. The lower energy band (λ_1) has a predominantly $^1[\pi(C{\equiv}CAr){\rightarrow}\pi^*(tpy)]$ character for the complexes in the "cop" conformation, and the higher energy band (λ_2) has mixed $^1[d_\pi(Pt){\rightarrow}\pi^*(Y_3tpy)]$ and $^1[\pi(C{\equiv}C){\rightarrow}\pi^*(Y_3tpy)]$ (C≡C is the carbon-carbon triple bond directly attached to the Pt ion) parentage for the complexes in the "per" conformation ("cop" and "per" refer to the conformations of the Pt^{II} complexes with the aryl rings coplanar and perpendicular to the Y_3tpy ligand, respectively). The alkyl acetylide analogues, $[Pt(Y_3tpy)(C{\equiv}CR)]^+$ (R = alkyl), show broad absorption bands at $\lambda\approx$400–430 and 420–490 nm for Y = tBu and Cl, respectively, which are assigned to a mixture of $^1[d_\pi(Pt){\rightarrow}\pi^*(Y_3tpy)]$ and $^1[\pi(C{\equiv}C){\rightarrow}\pi^*(Y_3tpy)]$ transitions. The emissions of $[Pt(Y_3tpy)(C{\equiv}CR)]^+$ (Y = tBu or Cl) are assigned to $^3[\pi(C{\equiv}CAr){\rightarrow}\pi^*(Y_3tpy)]$ excited states for R = aryl and $^3[d_\pi(Pt){\rightarrow}\pi^*(tpy)]/^3[\pi(C{\equiv}C){\rightarrow}\pi^*(Y_3tpy)]$ excited states for R = alkyl in CH_2Cl_2 at 298 K and in nBuCN (nBu = n-butyl) at 77 K. The chain length effect on the photophysical properties of $[Pt(Y_3tpy)(C{\equiv}CAr)]^+$ is discussed.

Results

Synthesis and characterization: The syntheses, elemental analyses, NMR spectroscopic data, and mass spectrometry data of salts of $[Pt(Y_3tpy)(C{\equiv}CAr)]^+$ are given in the Supporting Information. Cross-coupling reactions[9] of $[Pt(t\text{Bu}_3tpy)Cl]^+$[10] or $[Pt(Cl_3tpy)Cl]^+$[12] with HC≡CR[11] in the presence of a catalytic amount of CuI and diisopropylamine in CH_2Cl_2 or a mixture of CH_2Cl_2/CH_3CN (Me = methyl) gave complexes **1**–**22** with product yields ranging from 56 to 90%. The $[Pt(Cl_3tpy)Cl]^+$ complex, isolated as Cl^-, PF_6^- or $[Pt(dmso)Cl_3]^-$ salts, was first prepared by Horbert et al.[12] using $[Pt(dmso)_2Cl_2]$ as a precursor. Following the literature procedure, $[Pt(Cl_3tpy)Cl][Pt(dmso)Cl_3]$ was isolated and found to have a low solubility in common organic solvents, rendering its purification to be difficult. To circumvent this problem, $[Pt(Cl_3tpy)Cl]^+$ was prepared by using $[Pt(cod)Cl_2]$ (cod = 1,5-cyclooctadiene) as a precursor and was isolated as a OTf (OTf = triflate) salt. Since $[Pt(Cl_3tpy)Cl]OTf$ is more soluble in common organic solvents, it was used as a precursor for cross-coupling reactions with HC≡CR to give $[Pt(Cl_3tpy)(C{\equiv}CR)]^+$ for photophysical measurements.

All complexes are air- and moisture-stable (**1**–**22**) and were obtained as a yellow (**1**, **2a**, **3**–**6**, **8**–**10** and **20a**), orange (**2b**, **14** and **16**), reddish orange (**11**, **15** and **18**), brick red (**7a**, **13**, **20b**, **22**), brownish orange (**17** and **19**), purple (**12**, **7b**, **21a**) or dark green (**21b**) solids at room temperature. They were characterized by elemental analyses, IR and NMR (^{1}H, ^{13}C) spectroscopy, and MS. Additionally, **5** and **8** were characterized by ^{19}F NMR spectroscopy. The

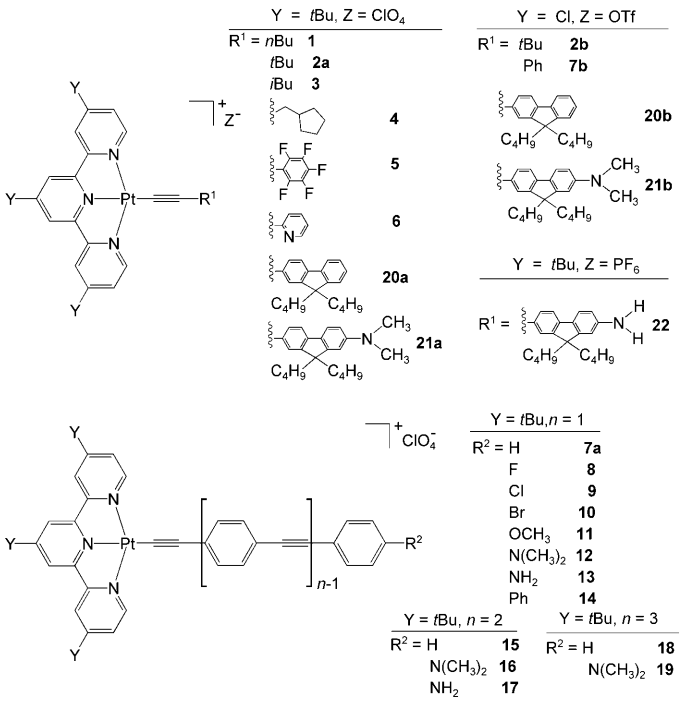

structures of **2a**, **4**–**6**, **7a** and **9**–**11** were determined by X-ray crystallography.

X-ray crystal structures: The crystal structures of **2a**, **4**, **5**·2 CH_3CN, **6**·CH_3CN, **7a**·2 CH_3CN, **9**·2 CH_3CN, **10**·2 CH_3CN, and **11**·2 CH_3CN were determined by X-ray crystallography (see Supporting Information, Tables S1 and S2, Figures S1–S8).[13] All of the complexes display one conformation in their crystal structures except **6**·CH_3CN, for which three different conformations were found (Figure S2 in Supporting Information). In each conformation, the platinum atom adopts a distorted square-planar geometry, which is comparable to the reported structures of terpyridyl platinum(II) complexes with σ-acetylide ligands.[1b,j,4b,9,10,14] The Pt–N(tBu$_3$tpy) distances are in the range of 1.930(8)–2.049(9) Å, as found in other platinum(II) terpyridine complexes.[1b,4b,14] The Pt–C(acetylide) distances are 1.914(2)–2.08(2) Å, which are similar to the reported values for $[Pt(tpy)(C{\equiv}CR)]^+$ (R = Ph, 1.98(1) Å;[14b] R = C_6H_4-$N(CH_3)_2$-4, 1.977(6) Å;[4b] R = C_6H_4-$N(CH_2CH_2OCH_3)_2$-4, 2.07(3) Å;[1b] and R = C_6H_4-NCS-4, 1.988(5) Å[14a]). The C≡C–C angles deviate slightly from the idealized angle of 180° (169.9(2)–178.7(7)°). The acetylenic aryl rings and the [Pt(Y$_3$tpy)] planes of **5**·2 CH_3CN, **7a**·2 CH_3CN, **9**·2 CH_3CN, **10**·2 CH_3CN, and **11**·2 CH_3CN are essentially coplanar, but, for **6**·CH_3CN, the dihedral angles between the acetylenic pyridyl and the tpy rings are in the range 56.6–70.9°. In the crystal structures of **2a**, **4**, **5**·2 CH_3CN, **7a**·2 CH_3CN, **9**·2 CH_3CN, **10**·2 CH_3CN and **11**·2 CH_3CN, the molecules are stacked in pairs in a head-to-tail fashion with Pt···Pt contacts > 4.0 Å, and the π···π separations between terpyridine units are in the range 3.472–3.588 Å, which would allow weak π···π interactions.[15] Intermolecular Pt···Pt contacts of 3.632 and 3.813 Å were found between the complex cations for all of the three conformations in the crystal structure of **6**·CH_3CN.

Resonance Raman spectroscopy: Resonance Raman (RR) spectra of **1** (R = nBu), **7a** (R = Ph), and **11** (R = C_6H_4-OCH_3-4) were obtained at λ_{ex} = 416 nm in CH_3CN and are depicted in Figure 1 a–c, respectively. For **1**, there are two fundamental vibrational modes and one overtone in its RR spectrum. The Raman band at 1550 cm^{-1} is assigned to nominal ν(C=C) and ν(C=N) stretching modes of tpy, and the one at 2134 cm^{-1} is attributed to ν(C≡C) of the acetylide ligand. In the cases of the aryl acetylide complexes **7a** and **11**, more fundamental vibrational modes appeared in the region of ≤1602 cm^{-1}, which are due to additional ν(C=C) and ν(C=N) stretching modes from the aryl group of arylacetylide ligands. Moreover, the fundamental vibrational stretches of ν(C≡C) of the aryl acetylides were found at 2120 cm^{-1} and 2121 cm^{-1} for **7a** and **11**, respectively.

Complex **11** was also excited at its lowest energy absorption band at 502.9 nm in CH_3CN (Figure 1 d).The resonance Raman spectrum of **11** obtained at λ_{ex} = 502.9 nm is different from that obtained at λ_{ex} = 416 nm. When **11** was irradiated at 502.9 nm, the RR intensity at 2121 cm^{-1} is almost double that of the 1300–1600 cm^{-1} bands; however, when **11** is irradiated at 416 nm, the RR intensity at 2121 cm^{-1} is almost half that of the 1300–1600 cm^{-1} bands.

Electronic absorption spectroscopy: The UV/Visible spectral data of **1**–**22** in CH_2Cl_2 are listed in Table 1. All of the complexes exhibit intense absorption bands at λ_{max} ≤380 nm with $\varepsilon \geq 10^4$ $dm^3mol^{-1}cm^{-1}$ and less intense broad bands at λ_{max} > 380 nm with ε values in the order of 10^3 $dm^3mol^{-1}cm^{-1}$. At λ_{max} > 380 nm, there are two partially overlapping bands (labeled λ_1 and λ_2 for the lower and higher energy regions, respectively). The main features of these two absorption bands are affected by: 1) substituents on both acetylide and tpy ligands of $[Pt(Y_3tpy)(C{\equiv}CR)]^+$ (Y = tBu or Cl, R = alkyl or aryl); 2) chain length n of aryl acetylide ligand of $[Pt(tBu_3tpy)\{C{\equiv}C(C_6H_4C{\equiv}C)_{n-1}C_6H_4$-X-4$\}]^+$ (n = 1–3: X = H or $N(CH_3)_2$; n = 1–2, X = NH_2); and 3) the addition of acid to $[Pt(tBu_3tpy)\{C{\equiv}C(C_6H_4C{\equiv}C)_{n-1}C_6H_4$-$NX_2-4\}]^+$ (n = 1–2, X = H; n = 1–3, X = CH_3) (these points will systematically be discussed below). All comparisons are based on the absorption spectra measured in CH_2Cl_2.

Substituent effect of $[Pt(Y_3tpy)(C{\equiv}CR)]^+$ (Y=tBu or Cl, R= alkyl or aryl): At the spectral region with λ > 380 nm, the absorption spectra of the alkyl–acetylide–platinum(II) complexes bearing tBu$_3$tpy ligands measured in CH_2Cl_2 show two partially overlapping absorption bands with broad peak maxima at λ_{max} = 403, 428 nm for **1** (R = nBu); 400, 429 nm for **2a** (R = tBu); 403, 428 nm for **3** (R = isobutyl (iBu)); and 404, 428 nm for **4** (R = CH_2cyp; cyp = cyclopentane). The aryl–acetylide complexes with the substituents R = Ph (**7a**), C_6H_4-F-4 (**8**), C_6H_4-Cl-4 (**9**), C_6H_4-Br-4 (**10**) also show two broad overlapping absorption maxima at λ_1 = 461–464 nm

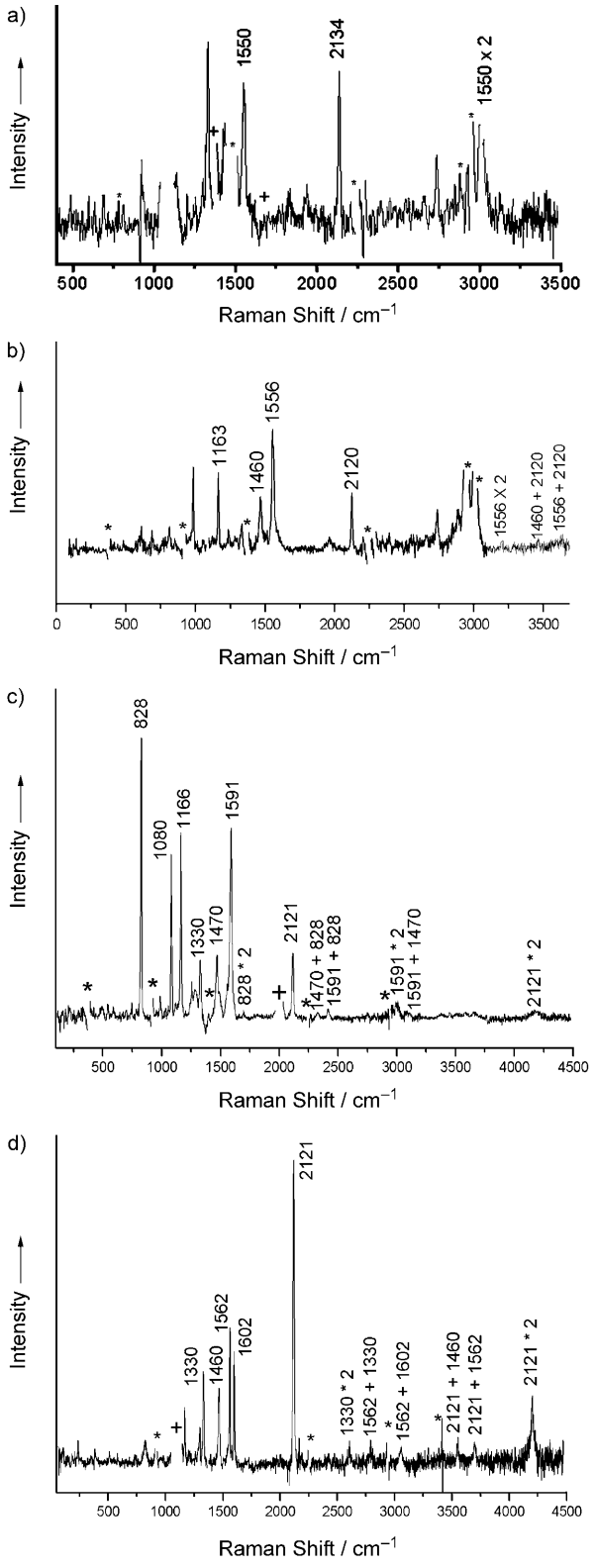

Figure 1. a) RR spectrum of **1** with $\lambda_{ex}=416$ nm in CH_3CN at 298 K. b) RR spectrum of **7a** with $\lambda_{ex}=416$ nm in CH_3CN at 298 K. c) RR spectrum of **11** with $\lambda_{ex}=416$ nm in CH_3CN at 298 K. d) RR spectrum of **11** with $\lambda_{ex}=502.9$ nm in CH_3CN at 298 K (solvent subtraction and background correction are marked by * and +, respectively).

and $\lambda_2=411$–413 nm. For the complexes with aryl–acetylide ligands that have electron-withdrawing substituents, $\lambda_1=413$ nm and $\lambda_2=383$ nm for **5** ($R=C_6F_5$) and $\lambda_1=412$ nm and $\lambda_2=389$ nm for **6** (R = Py; Py = pyridine), these λ_1 and λ_2 values are $\approx 2720\ cm^{-1}$ and $\approx 1690\ cm^{-1}$, respectively, higher in energy than those of **7a**. With electron-donating substituents $R=C_6H_4$-OCH_3-4 (**11**), C_6H_4-$N(CH_3)_2$-4 (**12**), C_6H_4-NH_2-4 (**13**), C_6H_4-Ph-4 (**14**), -(DBF)-H (**20a**), -(DBF)-$N(CH_3)_2$ (**21**), -(DBF)-NH_2 (**22**), λ_1 and λ_2 become distinctly separated with λ_1 at 476–577 nm and λ_2 at 404–413 nm (DBF = 9,9'-di-*n*-butyl-9H-fluorene). The λ_1 of **11**–**14** and **20a**–**22** show a significant redshift from **7a** with a span in values as much as $3920\ cm^{-1}$ and decreases in the order: **14** ($R=C_6H_4$-Ph-4; $21\,010\ cm^{-1}$) > **11** (C_6H_4-OCH_3-4; $20\,410\ cm^{-1}$) > **20a** (-(DBF)-H; $20\,160\ cm^{-1}$) > **13** (C_6H_4-NH_2-4; $19\,230\ cm^{-1}$) > **22** (-(DBF)-NH_2; $18\,800\ cm^{-1}$) > **21a** (-(DBF)-$N(CH_3)_2$; $17\,950\ cm^{-1}$) > **12** (C_6H_4-$N(CH_3)_2$-4; $17\,640\ cm^{-1}$). (The UV/Vis absorption spectra are shown in the Supporting Information, Figure S9.) The λ_2 of **11**–**14** and **20a**–**22** are insensitive to the *para*-substituent of the aryl–acetylide ligands. In general, both λ_1 and λ_2 of the Cl_3tpy series of R = *t*Bu, **2b**; Ph, **7b**; -(DBF)-H, **20b**; and -(DBF)-$N(CH_3)_2$, **21b** demonstrate a redshift by as much as $\approx 2330\ cm^{-1}$ from the corresponding *t*Bu_3tpy series (**2a**, **7b**, **20a**, and **21a**). (The UV/Vis absorption spectra of **2a** (Y = *t*Bu, R = *t*Bu) and **2b** (Y = Cl, R = *t*Bu) in CH_2Cl_2 are given in Supporting Information, Figure S10.)

The solvent effect on the UV/Vis absorption spectra of **5**, **7a**, **11**–**13** and **21b** was examined. (Their UV/Vis absorption data are listed in Supporting Information, Table S3.) A significant solvatochromic effect on the absorption bands at both $\lambda_{max}<380$ nm and λ_2 was not observed, and λ_1 shows negative solvatochromism. Figure 2 shows the UV/Vis absorption spectra of **7a** in various solvents; the largest span of λ_1 is $2840\ cm^{-1}$ and was observed by changing the solvent from CH_2Cl_2 to MeOH.

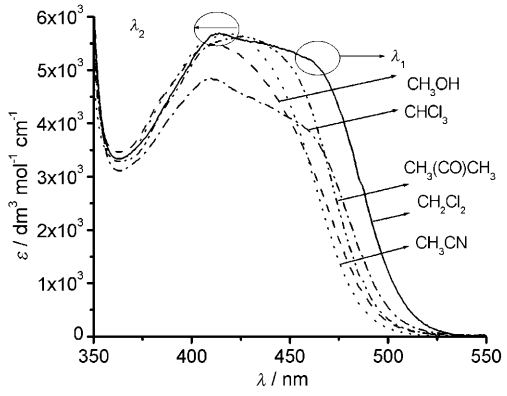

Figure 2. UV/Vis absorption spectra of **7a** in the 350–550 nm range in various solvents at 298 K (concentration 2×10^{-5} mol dm^{-3}).

[Pt(tBu$_3$tpy){C≡C(C$_6$H$_4$C≡C)$_{n-1}$C$_6$H$_4$-X-4}]$^+$ (n=1–3: X=H or N(CH$_3$)$_2$; n=1–2, X=NH$_2$) with aryl–acetylide ligands that have different chain lengths: Figures 3 and 4 show the

Table 1. Spectroscopic data of $[Pt(Y_3tpy)(C{\equiv}CR)]^+$ **1**–**22**.

Complex (Y, R)	Absorption λ_{max} [nm] (ε [$dm^3 mol^{-1} cm^{-1}$]	Emission in fluid solution at 298 K[a]: λ_{max} [nm] (τ_0 [μs]; ϕ_{em}[b]; k_q [1×10^8 $M^{-1} s^{-1}$]	Glassy emission at 77 K: λ_{max} [nm] (τ_0 [μs])[c]	Solid state emission at 298 K: λ_{max} [nm] (τ_0 [μs])[d]	Solid state emission at 77 K: λ_{max} [nm] (τ_0 [μs])[d]
1 (*t*Bu, *n*Bu)	287 (28760), 316 (20320), 326 (16770), 341 (17800), 403 (sh, 4680), 428 (5540)	548 (2.7); 0.32; 2.7	*499* (9.2), 534 (sh, 8.9)	541 (1.3)	508 (2.2), 541 (3.6), 577 (sh, 4.2)
2a (*t*Bu, *t*Bu)	287 (27660), 317 (19850), 325 (16970), 341 (17360), 400 (sh, 5410), 429 (6390)	547 (3.2); 0.44; 5.5	*498* (8.4), 530 (8.0)	*545* (1.3), 583 (sh, 4.0)	507 (1.1), *540* (1.9), 583 (4.0)
2b (Cl, *t*Bu)	256 (36180), 271 (sh, 30610), 310(sh, 12200), 324 (18240), 345 (7060), 422 (sh, 3840), 453 (4050), 483 (sh, 2650)	595 (0.45); 0.012; 16.9	*527* (7.15), 564 (sh, 7.20)	605 (0.37)	570 (sh, <0.1), *647* (1.65)
3 (*t*Bu, *i*Bu)	287 (29080), 316 (20740), 325 (17600), 341 (18530), 403 (sh, 4940), 428 (5840)	547 (3.0); 0.35; 1.7	*499* (9.0), 533 (8.7)	496 (sh), *529* (0.3), 563 (sh)	*492* (1.7), 531 (2.3), 570 (sh, 3.7)
4 (*t*Bu, CH_2cyp)	287 (28350), 316 (19840), 323 (17220), 341 (17450), 404 (sh, 4530), 428 (5190)	547 (3.0); 0.33; 1.4	*499* (9.3), 534 (9.7)	524 (0.9)	*509* (4.0), 545 (3.8), 585 (sh, 3.9)
5 (*t*Bu, C_6F_5)	286 (33890), 312 (19730), 323 (17630), 338 (19450), 383 (sh, 5070), 413 (6990)	524 (4.6); 0.55; 4.0	*486* (12.3), 519 (11.5), 614 (sh, 2.3)	634 (0.4)	640 (1.1)
6 (*t*Bu, Py)	287 (35700), 314 (19840), 323 (17380), 339 (17580), 389 (sh, 5380), 412 (6180)	545 (6.4); 0.61; 6.3	*484* (9.3), 520 (9.7)	546 (sh, 0.2), *620* (0.3)	*533* (6.0), 563 (sh, 5.3), 629 (sh, 2.0)
7a (*t*Bu, Ph)	285 (29570), 315 (19340), 325 (16770), 340 (16500), 413 (5950), 464 (sh, 5980)	587 (3.6); 0.18; 2.5	*526* (12.3), 608 (sh)	545 (sh, 0.2), *656* (0.2)	513, 590 (sh, 5.9), *671* (2.0)
7b (Cl, Ph)[a]	268 (sh, 36530), 319 (10050), 341 (7590), 420 (sh, 2620), 476 (sh, 2520) (CH_3CN)	635 (0.09); <0.01; n.d.[e]	insoluble	700 (<0.1)	745 (0.50)
8 (*t*Bu, C_6H_4-F-4)	286 (29900), 315 (20060), 325 (17270), 340 (17410), 412 (5640), 461 (sh, 5260)	588 (2.9); 0.14; 4.3	528 (13.2)	*515* (0.7), 553 (1.0), 590 (sh, 1.4)	*515* (3.0), 549 (6.3), 590 (sh, 7.4)
9 (*t*Bu, C_6H_4-Cl-4)	284 (48275), 315 (27480), 326 (24120), 340 (18830), 411 (5860), 462 (sh, 5530)	580 (4.4); 0.17; 6.3	526 (13.1)	515 (sh, 0.3), *600* (1.0)	523 (0.5), *597* (4.6)
10 (*t*Bu, C_6H_4-Br-4)	286 (39340), 314 (18590), 325 (16080), 340 (15770), 413 (5550), 461 (sh, 5430)	578 (4.0); 0.23; 4.2	523 (14.6)	518 (sh), *650* (0.2)	519, *666* (0.7)
11 (*t*Bu, C_6H_4-OCH_3-4)	284 (40650), 314 (19160), 324 (17510), 339 (15570), 383 (sh, 3650), 413 (4540), 490 (5320)	647 (<0.01); n.d.; n.d.	563 (12.2)	640 (0.6)	*620* (5.4), 660 (2.4)
12 (*t*Bu, C_6H_4-N-$(CH_3)_2$-4)	288 (47090), 296 (41170), 312 (33040), 337 (17960), 385 (sh, 3550), 405 (3790), 567 (4560)	541 (<0.01); n.d.; n.d., 535[f]	nonemissive	nonemissive	740 (<0.1)
13 (*t*Bu, C_6H_4-NH_2-4)	287 (60360), 312 (26720), 323 (22180), 338 (18860), 406 (5040), 520 (5700);	600 (<0.01); n.d.; n.d., 550[f]	nonemissive	nonemissive	768 (<0.1)
14 (*t*Bu, C_6H_4-Ph-4)	287 (53610), 337 (sh, 14600), 412 (4860), 476 (5330)	607 (0.70);0.04; 16.8[g]	*531* (12.1), 568 (11.8), 589 (sh, 8.76)	611 (0.55)	*585* (4.79), 620 (sh, 3.26)
15 (*t*Bu, $C_6H_4C{\equiv}$CPh)	288 (48120), 312 (62770), 329 (55250), 411 (6190), 469 (6766);	600 (0.96); 0.048; 3.6	*537* (35.8), 577 (28.3)	610 (0.5)	*581* (3.8), 621 (4.1)
16(*t*Bu, $C_6H_4C{\equiv}CC_6H_4$-N$(CH_3)_2$-4)	286 (49300), 298 (sh, 40900), 316 (43300), 342 (60490), 359 (sh, 53240), 411 (sh, 13210), 491 (7870)	520 (0.37); 0.04; n.d., 587[f]	550 (34.9)	723 (<0.1)	718 (<0.1)
17 (*t*Bu, $C_6H_4C{\equiv}CC_6H_4$-NH_2-4)	288 (39900), 316 (53650), 327 (58270), 340 (57480), 389 (6510), 409 (6550), 483 (6930)	600 (<0.01); n.d.; n.d., 586[f]	*551* (36.4); 593 (sh, 18.6)	nonemissive	644 (<0.1)
18 (*t*Bu, $C_6H_4C{\equiv}CC_6H_4C{\equiv}$CPh)	287 (34330), 326 (sh, 66520), 335 (70400), 358 (sh, 49500), 411 (6960), 471 (sh, 7530)	604 (0.87); 0.055; 1.1	*550* (153.7), 587 (162.3), 620 (2.33)	634 (0.30)	*621* (4.4), 668 (sh, 1.7), 690 (sh, 1.0)
19 (*t*Bu, $C_6H_4C{\equiv}CC_6H_4C{\equiv}CC_6H_4$-N-$(CH_3)_2$-4)	286 (31000), 315 (sh, 38330), 342 (49000), 360 (41960), 480 (sh, 5950)	601 (0.90); 0.012; 36.8[g]	*568* (273), 606 (sh, 295.6), 642 (sh, 2.14)	720 (<0.1)	707 (0.22)
20a (*t*Bu, -(DBF)-H)[h]	288 (34820), 303 (34910), 314 (34310), 327 (39740), 395 (sh, 3810), 412 (4030), 496 (4920)	642 (<0.01); n.d.; n.d.	549 (16.0)	589 (0.52)	*556* (7.23), 594 (sh, 6.81)
20b (Cl, -(DBF)-H)	274 (33780), 289 (34220), 300 (34140), 323 (40740), 342 (sh, 12760), 393 (sh, 3180), 420 (3940), 440 (sh, 3780), 549 (4280)	nonemissive	607 (7.43), *701*[i] (1.64)	*665* (0.26), 694 (sh, 0.25)	*657* (2.44), 705 (sh, 1.71)
21a (*t*Bu, -(DBF)-N$(CH_3)_2$)	270 (sh, 35100), 284 (sh, 27960), 340 (45510), 356 (sh, 42050), 411 (sh, br, 6960), 557 (5650)	nonemissive	nonemissive	608 (<0.1)	600 (sh), *646* (0.33), 706 (sh)
21b (Cl, -(DBF)-N$(CH_3)_2$)	254 (sh, 47820), 270 (sh,44480), 326 (41590), 345 (44340), 359 (44190), 421 (sh, 6190), 640 (4410)	undetectable[j]	undetectable[j]	undetectable[j]	undetectable[j]

Table 1. (Continued)

Complex (Y, R)	Absorption λ_{max} [nm] (ε [$dm^3 mol^{-1} cm^{-1}$]	Emission in fluid solution at 298 K[a]: λ_{max} [nm] (τ_0 [μs]; ϕ_{em}[b]; k_q [$1\times10^8 M^{-1} s^{-1}$]	Glassy emission at 77 K: λ_{max} [nm] (τ_0 [μs])[c]	Solid state emission at 298 K: λ_{max} [nm] (τ_0 [μs])[d]	Solid state emission at 77 K: λ_{max} [nm] (τ_0 [μs])[d]
22 (*t*Bu, -(DBF)-NH_2)	270 (sh, 20200), 288 (19450), 316 (30920), 341 (32440), 397 (sh, br, 3710), 532 (3560)	nonemissive	nonemissive	658 (<0.1)	647 (0.43)

[a] Room-temperature emission maxima in degassed CH_2Cl_2 at complexes concentrations of 2×10^{-5} mol dm^{-3} with $\lambda_{ex}=430$ nm unless otherwise stated. [b] The luminescence quantum yield ϕ_{em} was measured at room temperature using $[Ru(bpy)_3][PF_6]_2$ in degassed CH_3CN as a standard. [c] Emission band maxima in glassy *n*BuCN with $\lambda_{ex}=430$ nm at complexes concentrations of 1×10^{-5} mol dm^{-3}, emission maxima are in *italics*. [d] $\lambda_{ex}=430$ nm, emission maxima are in *italics*. [e] Measured at 2×10^{-5} mol dm^{-3}, in CH_3CN, n.d. = not detected. [f] Addition with a few drops of CF_3COOH. $\lambda_{ex}=405$, 409, 400 and 480 nm for **12**, **13**, **16**, and **17** respectively. [g] $\lambda_{ex}=475$ and 480 nm for **14** and **19**, respectively. [h] DBF = 9,9'-di-*n*-butyl-9*H*-fluorene. [i] For comparison of ^{3}LLCT emissive-state in the discussion section, the emission maxima concerns $\lambda=607$ nm, since λ_{max} at 701 nm is concentration dependent. [j] Due to the instrumental limitation, $\lambda>900$ nm is undetectable.

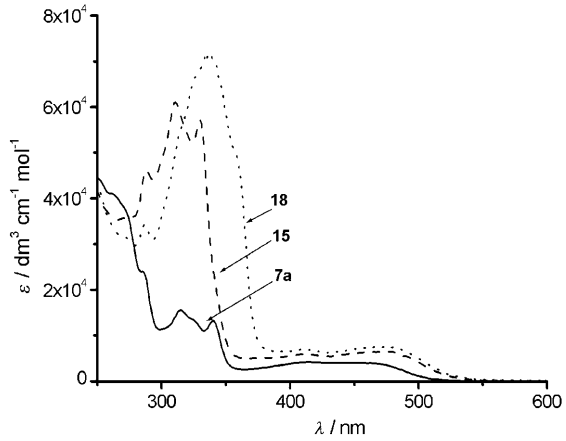

Figure 3. UV/Vis absorption spectra of $[Pt(tBu_3tpy)\{C\equiv C(C_6H_4\text{-}C\equiv C)_{n-1}Ph\}]ClO_4$ ($n=1$, **7a**; $n=2$, **15**; and $n=3$, **18**) in CH_2Cl_2 at 298 K (concentration $=2\times10^{-5}$ mol dm^{-3}).

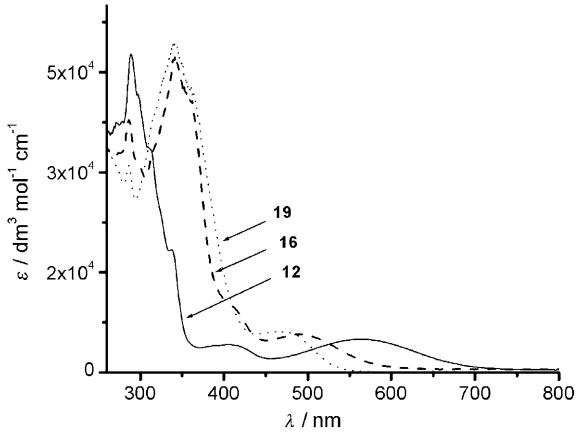

Figure 4. UV/Vis absorption spectra of $[Pt(tBu_3tpy)\{C\equiv C(C_6H_4\text{-}C\equiv C)_{n-1}C_6H_4\text{-}N(CH_3)_2\text{-}4\}]ClO_4$ ($n=1$, **12**; $n=2$, **16**; and $n=3$, **19**) in CH_2Cl_2 at 298 K (concentration $=2\times10^{-5}$ mol dm^{-3}).

UV/Vis absorption spectra of $[Pt(tBu_3tpy)\{C\equiv C(C_6H_4\text{-}C\equiv C)_{n-1}C_6H_4\text{-X-4}\}]^+$ with X = H and $N(CH_3)_2$ ($n=1$–3), respectively. The UV/Vis absorption spectra of $[Pt(tBu_3tpy)\{C\equiv C(C_6H_4C\equiv C)_{n-1}C_6H_4\text{-X-4}\}]^+$ (X = NH_2, $n=1$–2) are given in the Supporting Information (Figure S11). Complexes **7a** ($n=1$), **15** ($n=2$), and **18** ($n=3$) of the X = H series display spectroscopic properties different from those of **12** ($n=1$), **16** ($n=2$), and **19** ($n=3$) of the X = $N(CH_3)_2$ series and from those of **13** ($n=1$) and **16** ($n=2$) of the X = NH_2 series. The λ_1 value of the X = H series shows a slight redshift with increasing chain length: **7a** ($n=1$, 21550 cm^{-1}, 464 nm) > **15** ($n=2$, 21320 cm^{-1}, 469 nm) > **18** ($n=3$, 21230 cm^{-1}, 471 nm). Conversely, λ_1 shows a blueshift with increase in n for the X = $N(CH_3)_2$ and NH_2 series: $\approx$3190 cm^{-1} when changing n from 1 to 3 for X = $N(CH_3)_2$ and $\approx$1470 cm^{-1} when changing n from 1 to 2 for the X = NH_2 series.

Effect of acid on the electronic transitions of $[Pt(tBu_3tpy)\{C\equiv C(C_6H_4C\equiv C)_{n-1}C_6H_4\text{-X-4}\}]^+$ (n=*1–2: X=*NH_2 *or* n=*1–3: X=*$N(CH_3)_2$*):* There is a distinct color change from dark purple ($n=1$, X = $N(CH_3)_2$, **12**), reddish orange ($n=1$, X = NH_2, **13**; $n=2$: X = $N(CH_3)_2$, **16** and X = NH_2, **17**), or reddish brown ($n=3$: X = $N(CH_3)_2$, **19**) to bright yellow upon addition of a few drops of neat CF_3COOH to solutions of the Pt^{II} complexes. As depicted in Figure 5, a significant blueshift of the lowest energy absorption maxima (λ_1) of the amine substituted aryl–acetylide complexes **12**, **13**, **16**, **17** and **19** was observed after addition of neat CF_3COOH. A similar finding has previously been reported for terpyridyl Pt^{II} complexes containing amino substituted aryl–acetylide ligands.[1a,b, 2a,4] The λ_1 shows a blueshift from 567 to 412 nm and from 520 nm to 409 nm for **12** (X = $N(CH_3)_2$, span of 6640 cm^{-1}) and **13** (X = NH_2, span of 5220 cm^{-1}), respectively, with a growth in the absorption maxima intensity around 380–415 nm after the addition of acid. Similarly, λ_1 of **16** ($n=2$, X = $N(CH_3)_2$) and **17** ($n=2$, X = NH_2) demonstrate a blueshift from 491 and 483 nm to 448 and 446 nm, respectively, (1950 cm^{-1} shift for **16** and 1720 cm^{-1} shift for **17**), though the shift is smaller than the corresponding values for the $n=1$ counterparts, that is, **12** (X = $N(CH_3)_2$) and **13** (X = NH_2). Interestingly, both the absorption energy and absorptivity of the lowest absorption band (λ_1) for **19** ($n=3$, X = $N(CH_3)_2$) are essentially unperturbed upon addition of a few drops of neat CF_3COOH.

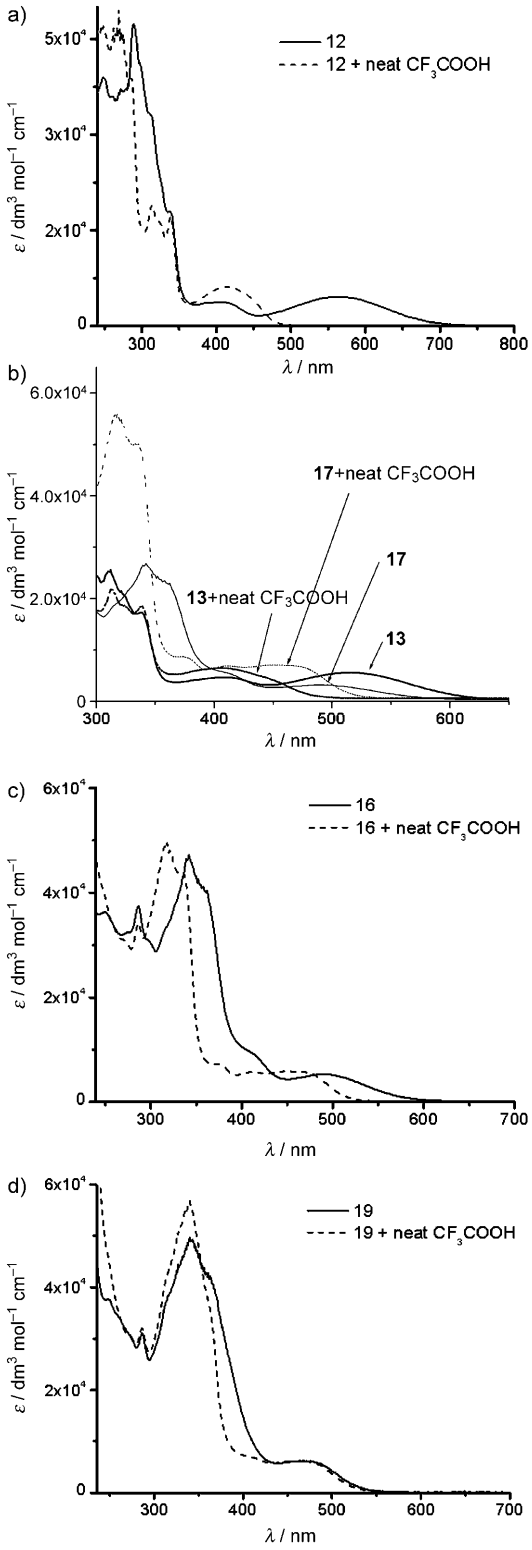

Figure 5. a) UV/Vis absorption spectra of **12** in CH_2Cl_2 before and after addition of a few drops of neat CF_3COOH at 298 K. b) UV/Vis absorption spectra of **13** and **17** in CH_2Cl_2 before and after addition of a few drops of neat CF_3COOH at 298 K. c) UV/Vis absorption spectra of **16** in CH_2Cl_2 before and after addition of a few drops of neat CF_3COOH at 298 K. d) UV/Vis absorption spectra of **19** in CH_2Cl_2 before and after addition of a few drops of neat CF_3COOH at 298 K (concentration 2×10^{-5} mol dm^{-3}).

Emission spectroscopy: The emission data of $[Pt(Y_3tpy)(C{\equiv}CR)]^+$ (Y = *t*Bu or Cl, R = alkyl or aryl) **1**–**22** are listed in Table 1. The emission lifetimes are in the microsecond range, revealing that the emitting states are of triplet parentage. We will focus mainly on the solution-state emission properties of complexes **1**–**22** at both 298 and 77 K.

*Substituent effect of $[Pt(Y_3tpy)(C{\equiv}CR)]^+$ (Y=t**Bu or Cl**, R= alkyl or aryl)*: For the tBu$_3$tpy series, the alkyl–acetylide complexes (**1**–**4**, except **2b**) emit at 547 (R = *t*Bu, **2a**; *i*Bu, **3**; and CH_2cyp, **4**), and 548 nm (*n*Bu, **1**) with emission quantum yields of 0.32–0.44 in degassed CH_2Cl_2 at 298 K. Conversely, the emission maxima of the aryl–acetylide complexes (**7a**, **8**-**10**, and **14** with R = Ph, C_6H_4-F-4, C_6H_4-Cl-4, C_6H_4-Br-4, C_6H_4-Ph-4, respectively), range from 578 to 607 nm and show a redshift from those of the alkyl–acetylide complexes. The emission quantum yields of the aryl–acetylide complexes (**7a**, **8**–**10**, and **14** with $\phi_{em}=0.04$–0.23) are lower than those of the alkyl–acetylide complexes **1**–**4** (except **2b**). This could be accounted for by the energy-gap law,[16] since these last complexes emit at a higher energy. Consistent with the UV/Vis absorption spectral data of **5** and **6** (R = C_6F_5 and Py, respectively), in which their absorption maxima, λ_1, are at higher energies than that of **7a** (R = Ph), the emission maxima of the former two complexes ($\lambda_{max}=524$ and 545 nm for **5** and **6**, respectively) show a blueshift from that of the latter ($\lambda_{max}=587$ nm). In the cases of electron-donating substituents, R = C_6H_4-OCH_3-4 (**11**), amine-substituted aryl groups (**12**, **13**, **16**, **17**, **19**, **21a**, and **22**), fluorene-substituted aryl groups (**20a**), these aryl–acetylide–platinum(II) complexes are nonemissive ($\phi_{em}<0.01$) in degassed CH_2Cl_2 at ambient temperature. This phenomenon has similarly been reported in other terpyridine–Pt^{II} complexes with nonsubstituted tpy ligands bearing electron-donating aryl–acetylide ligands.[1b,2a,4,14] For the Cl_3tpy series, **2b** (R = *t*Bu) exhibits an emission at $\lambda_{max}=595$ nm ($\phi_{em}=0.012$), and **7b** (R = Ph) and **20b** (R = DBF) are nonemissive ($\phi_{em}<0.01$) in degassed CH_2Cl_2 at 298 K.

All of the $[Pt(t\text{Bu}_3\text{tpy})(C{\equiv}CR)]^+$ (R = alkyl or aryl) complexes are emissive in glassy *n*BuCN at 77 K (concentration 1×10^{-5} mol dm^{-3}) except **12**, **13**, **21a**, and **22**, which have amine substituted aryl–acetylide ligands. The alkyl–acetylide complexes **1**–**4** (except **2b**) show emission maxima at 498–499 nm, which are at higher energies than those of the aryl–acetylide complexes with the exception of **5** and **6**. The emission maxima of the aryl–acetylide complexes **5**, **6**, **7a**, **8**–**11**, **14**, and **20a** are in the range of 484–567 nm with the emission energies following the order: **6** (20660 cm^{-1}, R = Py) > **5** (20580 cm^{-1}, R = C_6F_5) > **10** (19120 cm^{-1}, R = C_6H_4-Br-4) > **7a** (19010 cm^{-1}, R = Ph) ≈ **9** (19010 cm^{-1}, R = C_6H_4-Cl-4) > **8** (18940 cm^{-1}, R = C_6H_4-F-4) > **14** (18830 cm^{-1}, R = C_6H_4-Ph-4) > **20a** (18210 cm^{-1}, R = -(DBDF)-H) > **11** (17760 cm^{-1}, R = C_6H_4-OCH_3-4). Changing the tBu$_3$tpy to Cl_3tpy leads to a redshift in the emission energy. For instance, from **2a** to **2b** (R = *t*Bu), the redshift in emission energies are ≈1540 and 1070 cm^{-1} in degassed CH_2Cl_2 at 298 K and in *n*BuCN at 77 K, respectively.

[Pt(tBu$_3$tpy){C≡C(C$_6$H$_4$C≡C)$_{n-1}$C$_6$H$_4$-X-4}]$^+$ (n=1–3: X=H or N(CH$_3$)$_2$; n=1–2, X=NH$_2$) with different chain lengths: The effect of the chain length n of aryl–acetylide ligands on the emission properties of [Pt(tBu$_3$tpy){C≡C(C$_6$H$_4$-C≡C)$_{n-1}$C$_6$H$_4$-X-4}]$^+$ (n=1–3: X=H and N(CH$_3$)$_2$; n=1–2: NH$_2$) was examined. For [Pt(tBu$_3$tpy){C≡C(C$_6$H$_4$-C≡C)$_{n-1}$Ph}]$^+$ (n=1 (**7a**), n=2 (**15**), or n=3 (**18**)) complexes, their emission bands recorded in CH_2Cl_2 are broad and structureless, and the emission λ_{max} shows a slight redshift from 587 to 604 nm as n increases from 1 to 3 at 298 K (Figure 6). The emission energies fall in the order: **7a** (17040 cm^{-1}, n=1) > **15** (16670 cm^{-1}, n=2) > **18** (16560 cm^{-1}, n=3). At 77 K and in glassy nBuCN, **7a**, **15**, and **18**, display structured emission bands at λ_{max}=526, 537, and 550 nm, respectively (Figure 7).

For the [Pt(tBu$_3$tpy){C≡C(C$_6$H$_4$C≡C)$_{n-1}$C$_6$H$_4$-NH$_2$-4}]$^+$ series, **13** (n=1) is nonemissive ($\phi_{em}<0.01$) in CH_2Cl_2 at 298 K and in glassy nBuCN at 77 K, but **17** (n=2) is emissive at λ_{max}=551 nm (τ=36 μs) in glassy nBuCN at 77 K. For the [Pt(tBu$_3$tpy){C≡C(C$_6$H$_4$C≡C)$_{n-1}$C$_6$H$_4$-N(CH$_3$)$_2$-4}]$^+$ series, **12** (n=1) is nonemissive ($\phi_{em}<0.01$) in CH_2Cl_2 at 298 K and in glassy nBuCN at 77 K, but **16** (n=2) and **19** (n=3) are emissive under similar conditions. Complex **16** emits at λ_{max}=507 (τ=0.4 μs, $\phi_{em}=4.0\times10^{-2}$) in CH_2Cl_2 at 298 K and at 550 nm (τ=35 μs) in nBuCN at 77 K, and complex **19** shows emission maxima at 601 (τ=0.9 μs, $\phi_{em}=1.2\times10^{-2}$) in CH_2Cl_2 at 298 K and 568 nm (τ=270 μs) in glassy nBuCN at 77 K.

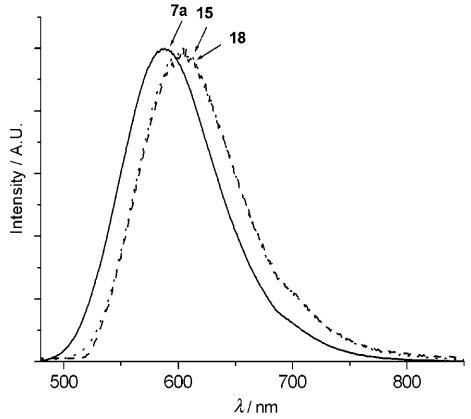

Figure 6. Emission spectra of [Pt(tBu$_3$tpy){C≡C(C$_6$H$_4$C≡C)$_{n-1}$Ph}]ClO$_4$ (n=1, **7a**; n=2, **15**; and n=3, **18**) in degassed CH_2Cl_2 at 298 K (λ_{ex}=430 nm, concentration 2×10^{-5} mol dm^{-3}).

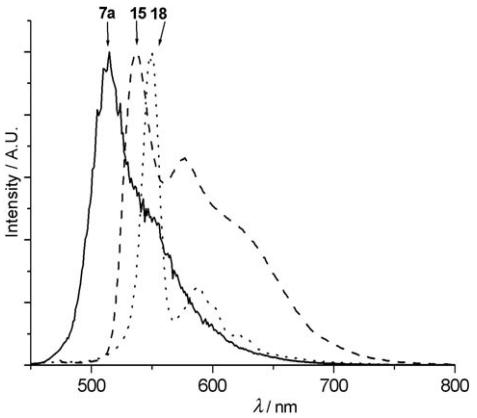

Figure 7. Emission spectra of [Pt(tBu$_3$tpy){C≡C(C$_6$H$_4$C≡C)$_{n-1}$Ph}]ClO$_4$ (n=1, **7a**; n=2, **15**; and n=3, **18**) in glassy nBuCN at 77 K (λ_{ex}=430 nm, concentration 1×10^{-5} mol dm^{-3}).

Effect of acid to the electronic transitions of [Pt(tBu$_3$tpy)-{C≡C(C$_6$H$_4$C≡C)$_{n-1}$C$_6$H$_4$-X-4}]$^+$ (n=1–2, X=NH$_2$; n=1–3, X=N(CH$_3$)$_2$: The emission intensities at λ_{max}=541 nm of **12** (X=N(CH$_3$)$_2$, n=1) and at $\lambda_{max}\approx$600 nm of **13** and **17** (X=NH$_2$, n=1 and 2, respectively) in degassed CH_2Cl_2 at 298 K increase upon addition of a few drops of neat CF_3COOH (see Figures S12, S13, and S14, respectively, in the Supporting Information). The emission energies of the protonated forms of **12**, **13**, and **17** show a blueshift (span 210–1520 cm^{-1}) from their respective nonprotonated ones. However, the emission of **16** (X=N(CH$_3$)$_2$; n=2) demonstrates a redshift from 520 to 587 nm by ≈2220 cm^{-1} after the addition of neat CF_3COOH, and **19** (X=N(CH$_3$)$_2$; n=3) emits at the same emission maximum (λ_{max}=601 nm) in the presence and absence of acids.

Calculations: DFT and TDDFT calculations were performed for the model complexes [Pt(H$_3$tpy)(C≡CR)]$^+$ (R=nPr (**1H**), Py (**6H**), Ph (**7aH**), and C$_6$H$_4$-N(CH$_3$)$_2$-4 (**12H**)), [Pt-(H$_3$tpy){C≡C(C$_6$H$_4$C≡C)$_{n-1}$Ph}]$^+$ (n=2 (**15H**) and n=3 (**18H**)), [Pt(H$_3$tpy){C≡C(C$_6$H$_4$C≡C)$_{n-1}$C$_6$H$_4$-N(CH$_3$)$_2$-4}]$^+$ (n=2 (**16H**) and n=3 (**19H**)), and [Pt(H$_3$tpy){C≡C(C$_6$H$_4$-C≡C)$_{n-1}$C$_6$H$_4$-N(CH$_3$)$_2$-4}]$^+$+H$^+$ (n=1 (**12H**+H$^+$), n=2 (**16H**+H$^+$), and n=3 (**19H**+H$^+$)) in order to understand the photophysical properties of [Pt(Y$_3$tpy)(C≡CR)]$^+$ (Y=tBu or Cl, R=alkyl or aryl). (The results are summarized in the Supporting Information, Table S5.) Here, we considered two extreme conformations as depicted in Figure 8: the H$_3$tpy plane and the aryl plane being coplanar ("cop") and perpendicular ("per") to each other, since the aryl rings of the aryl–acetylide complexes are free to rotate at room temperature. Comparison of the energies of spin-allowed singlet electronic transitions of these model complexes were performed to explore how the electronic absorption energies are affected by: 1) acetylide substituent of [Pt(H$_3$tpy)-(C≡CR)]$^+$ with R=nPr (**1H**), Py (**6H**), Ph (**7aH**), and C$_6$H$_4$-N(CH$_3$)$_2$-4 (**12H**); 2) the chain length n of [Pt(H$_3$tpy)-{C≡C(C$_6$H$_4$C≡C)$_{n-1}$C$_6$H$_4$-X-4}]$^+$ (n=1: (**7aH**), n=2: (**15H**), n=3: (**18H**); X=H and n=1: (**12H**), n=2: (**16H**), n=3: (**19H**); X=N(CH$_3$)$_2$); and 3) addition of acid to [Pt(H$_3$tpy)-{C≡C(C$_6$H$_4$C≡C)$_{n-1}$C$_6$H$_4$-N(CH$_3$)$_2$-4}]$^+$/+H$^+$ with different chain lengths n (n=1 (**12H**+H$^+$), n=2 (**16H**+H$^+$), and n=3 (**19H**+H$^+$)).

Substituent R of [Pt(H$_3$tpy)(C≡CR)]$^+$ (R=nPr, Py, Ph, and C$_6$H$_4$-N(CH$_3$)$_2$-4): The lowest allowed transition energies (f>0) obtained from TDDFT calculations for **1H**, **6H**, **7aH**, and **12H** with "cop" and "per" conformations in CH_2Cl_2, together with the experimental low-energy absorption maxima (λ_{max}>380 nm) measured in CH_2Cl_2 are listed

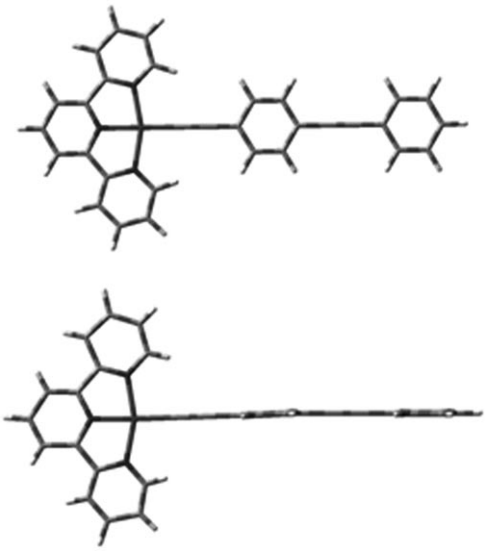

Figure 8. Geometries of "cop" (top) and "per" (bottom) conformations; **15H** is taken as an example here.

in the Supporting Information (Table S5). For **1H** (R = *n*Pr), there is a strong band ($f \approx 0.1$) derived from a HOMO→LUMO transition at $\lambda_{calcd} = 450$ and 451 nm for the "cop" and "per" conformations, respectively. When R changes from alkyl (*n*Pr) to aryl (Py, Ph, and C_6H_4-N(CH_3)$_2$-4) groups, the lowest spin-allowed singlet transitions for the "cop" and "per" conformations are derived from different electronic origins. The $\lambda_{calcd} = 473$–732 nm (span 7480 cm^{-1}) of the complexes with the "cop" conformations are assigned to the HOMO→LUMO transitions and show a redshift as the aryl group R becomes more electron-donating: **6H** (R = Py, 473 nm) < **7aH** (Ph, 512 nm) < **12H** (C_6H_4-N(CH_3)$_2$-4, 732 nm). This result is consistent with the experimental findings of λ_1 values: **6** (Py, 412 nm) < **7a** (Ph, 464 nm) < **12** (C_6H_4-N(CH_3)$_2$-4, 567 nm) with a span of 6640 cm^{-1}. On the other hand, at the "per" conformations, $\lambda_{calcd} = 409$–435 nm (span ≈ 1460 cm^{-1}) are assigned to the HOMO−1→LUMO transitions, which show a redshift to a lesser extent compared with those of the HOMO → LUMO transitions with the complexes at "cop" conformations when the electron-donating ability of the aryl group R increases. The small change of the HOMO−1→LUMO transition energy is comparable to the experimental findings of λ_2 (from 389 to 413 nm, span ≈ 1494 cm^{-1}; see Table S5 in the Supporting Information).

The HOMO of **1H** is different from that of **6H**, **7aH**, and **12H** in that it is an antibonding combination of ≈34–35% Pt(d_{xz}) and ≈47–48% π(C≡C) fragment orbitals for the complexes at both "cop" and "per" conformations. For the last three aryl–acetylide complexes with "cop" conformations, their HOMOs are predominantly the entire aryl–acetylide ligand in character, which increase from 71% with R = Py (**6H**) to 75% with R = Ph (**7aH**) and to 91% with R = C_6H_4-N(CH_3)$_2$-4 (**12H**) with decreasing admixture of Pt(d_{xz}) character. The HOMO energy increases since R is more electron-donating and this leads to a redshift in the HOMO→LUMO transition of the complex with the "cop" conformation (see Table S4 in the Supporting Information). The HOMO−1 of **6H**, **7aH** and **12H** with "per" conformations are antibonding combinations of ≈37–41% Pt(d_{xz}) and ≈44–46% π(C≡C) fragment orbitals, without involvement of the *para*-substituents in the aryl groups. Since the *para*-substituent of the aryl group does not have a significant effect on the HOMO−1 energy of **6H**, **7aH** and **12H**, the insignificant variation in the experimental λ_2 values at 389 nm (**6**, Py); 413 nm (**7a**, Ph); 405 nm (**12**, C_6H_4-N(CH_3)$_2$-4) could come from the HOMO−1→LUMO transition with "per" conformation. For both alkyl and aryl–acetylide complexes with "cop" and "per" conformations, the LUMOs are essentially of H_3tpy (89–91%: "cop" and 91–92%: "per") in character and the molecular orbital (MO) energies are invariant with the substituents R (R = *n*Pr (**1H**), Py (**6H**), Ph (**7aH**), and C_6H_4-N(CH_3)$_2$-4 (**12H**)). Thus, the lowest energy absorption band at $\lambda_{calcd} = 450$–451 nm for **1H** (R = alkyl) is an admixture of $^1[d_\pi(Pt) \rightarrow \pi^*(H_3tpy)]$/$^1[\pi(C{\equiv}C) \rightarrow \pi^*(H_3tpy)]$, and for **6H**, **7aH**, and **12H** (R = aryl), the $\lambda_{calcd} = 473$–732 nm are predominantly of $^1[\pi(C{\equiv}CAr) \rightarrow \pi^*(H_3tpy)]$ in character, and $\lambda_{calcd} = 409$–435 nm, being of similar nature to the lowest energy absorption bands of **1H**, could be described to have mixed $^1[d_\pi(Pt) \rightarrow \pi^*(H_3tpy)]$/$^1[\pi(C{\equiv}C) \rightarrow \pi^*(H_3tpy)]$ parentages.

[Pt(tBu_3tpy){C≡C(C_6H_4C≡C)$_{n-1}$$C_6H_4$-X-4}]$^+$ (n=1–3: X=H or N(CH_3)$_2$) with different chain lengths: The HOMO surfaces of [Pt(H_3tpy){C≡C(C_6H_4C≡C)$_{n-1}$$C_6H_4$-X-4}]$^+$ (X = H, *n* = 1 (**7aH**), *n* = 2 (**15H**), *n* = 3 (**18H**) and X = N(CH_3)$_2$, *n* = 1 (**12H**), *n* = 2 (**16H**), *n* = 3 (**19H**)) are shown in Tables 2 and 3, respectively. In agreement with the experimental findings for [Pt(*t*Bu_3tpy){C≡C(C_6H_4C≡C)$_{n-1}$Ph}]$^+$ with λ_1 = 464 nm (**7a**, *n* = 1), 469 nm (**15**, *n* = 2), and 471 nm (**18**, *n* = 3), the lowest calculated singlet transition energy shows a slight redshift from $\lambda_{calcd} = 512$ nm for *n* = 1 to 561 nm for *n* = 2 and to 576 nm for *n* = 3 with the "cop" conformation and is derived from a HOMO→LUMO transition. The HOMOs of [Pt(H_3tpy){C≡C(C_6H_4C≡C)$_{n-1}$Ph}]$^+$ are mainly

Table 2. The HOMO surfaces of the model complexes [Pt(H_3tpy){C≡C-(C_6H_4C≡C)$_{n-1}$Ph}]$^+$ (*n* = 1 (**7aH**), *n* = 2 (**15H**) and 3 (**18H**)) of partially optimized singlet ground state with the "cop" and "per" conformations.

7aH (*n* = 1)	**15H** (*n* = 2)	**18H** (*n* = 3)
"cop" conformation HOMO		
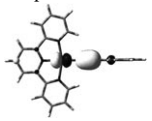	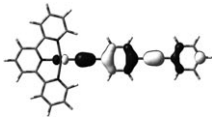	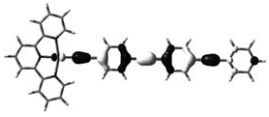
"per" conformation: HOMO−1[a]		
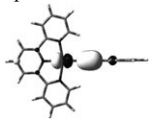	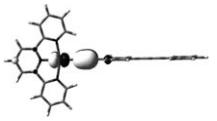	

[a] HOMO−2 for *n* = 3.

Table 3. The HOMO surfaces of the model complexes $[Pt(H_3tpy)\{C{\equiv}C(C_6H_4C{\equiv}C)_{n-1}C_6H_4\text{-}N(CH_3)_2\text{-}4\}]^+$ ($n=1$ (**12H**), $n=2$ (**16H**) and $n=3$ (**19H**)) at both optimized singlet ground state with "cop" and "per" conformations.

	12H ($n=1$)	**16H** ($n=2$)	**19H** ($n=3$)
"cop" conformation			
HOMO−1	–	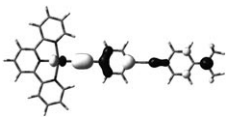	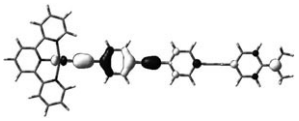
HOMO	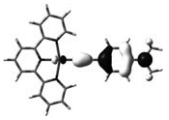	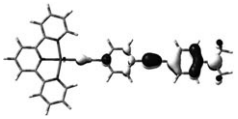	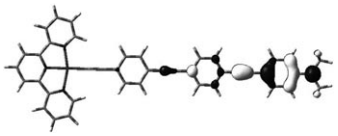
"per" conformation:			
HOMO-*n*	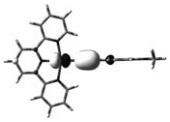	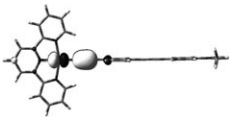	
HOMO	–	–	

antibonding combinations of π(C≡C) and Ar fragment orbitals (Ar = aryl rings on aryl–acetylide groups): **7aH** ($n=1$, 20% Pt, 35% C≡C, 40% Ar); **15H** ($n=2$, 9% Pt, 37% C≡C, 51% Ar); **18H** ($n=3$, 5% Pt, 38% C≡C, 55% Ar), whereas the LUMOs are all H_3tpy-based (90–91%) irrespective of the chain length n (see Table S4 in the Supporting Information). Since the HOMO is composed of p_π moieties of aryl–acetylide ligand delocalized over the entire chain, the number of nodes in the oligomeric aryl–acetylide ligand increases as n increases, leading to an increase in the HOMO energy. Thus, the calculated lowest absorption energy of **7aH**, **15H** and **18H** with "cop" conformations show redshifts as the chain length n increases and is assigned as $^1[\pi(C{\equiv}CAr){\rightarrow}\pi^*(H_3tpy)]$ transitions. With "per" conformations, the only allowed transitions for **7aH**, **15H**, and **18H** are derived from HOMO−1 (or HOMO−2 for $n=3$)→LUMO transitions, which slightly change from $\lambda_{calcd}=423$ to 418 nm as the chain length n increases from 1 to 3. The HOMO−1 (or HOMO−2 for $n=3$) of **7aH**, **15H**, and **18H** are similar to the HOMO of **1H**, consisting of antibonding combinations of $Pt(d_{xz})$ and π(C≡C) (directly attached to Pt) fragment orbitals and the LUMOs of **7aH**, **15H**, and **18H** are all H_3tpy-based irrespective of chain length n. Hence, this HOMO−1 (or HOMO−2 for $n=3$)→LUMO transition is assigned to mixed $^1[d_\pi(Pt){\rightarrow}\pi^*(H_3tpy)]/^1[\pi(C{\equiv}C){\rightarrow}\pi^*(H_3tpy)]$ transitions.

For **12H** ($n=1$), **16H** ($n=2$), and **19H** ($n=3$) with X = N-$(CH_3)_2$, their HOMOs with the complexes in the "cop" conformation are essentially localized on the C_6H_4-N$(CH_3)_2$-4 group with contributions of 77% ($n=1$), 67% ($n=2$) and 65% ($n=3$), and the LUMO and LUMO+1 are predominantly of H_3tpy character (see Table S4 in Supporting Information). The calculated lowest absorption band for the "cop" conformation shows a blueshift from $\lambda_{calcd}=732$ nm at $n=1$ (**12H**) to 714 nm for $n=2$ (**16H**) and to 683 nm at $n=3$ (**19H**). This band is derived from a HOMO→LUMO transition with $f>0.2$. There is another band of smaller oscillator strength ($f<0.02$), which was found to be HOMO→LUMO+1 in character and also shows a blueshift with increase in chain length n: $\lambda_{2(calcd)}=$ 598 nm for $n=1$; 566 nm for $n=2$; and 543 nm for $n=3$. Both calculated absorption bands are in accordance with the experimental trend of λ_1 of $[Pt(tBu_3tpy)\{C{\equiv}C(C_6H_4C{\equiv}C)_{n-1}C_6H_4\text{-}N(CH_3)_2\text{-}4\}]^+$ ($n=1$–3), which also shows a blueshift with increase in chain length n from 1 to 3. Thus, λ_1 is assigned to the $^1[\pi(C{\equiv}CAr){\rightarrow}\pi^*(H_3tpy)]$ transition. With $[Pt(H_3tpy)\{C{\equiv}C(C_6H_4C{\equiv}C)_{n-1}C_6H_4\text{-}N(CH_3)_2\text{-}4\}]^+$ (**12H**, **16H** and **19H**, $n=1$, 2 and 3, respectively, in "per" conformation), an allowed transition at $\lambda_{calcd}=413$–435 nm is assigned to HOMO−n→LUMO ($n=1$–3) transitions. These HOMO−n orbitals are essentially of the same character as the HOMO−1 (HOMO−2 for **18H**) for $[Pt(H_3tpy)\{C{\equiv}C(C_6H_4C{\equiv}C)_{n-1}Ph\}]^+$ (**7aH**, **15H**, and **18H**, $n=1$, 2 and 3, respectively) with "per" conformation, in other words, antibonding combinations of ≈37–39% $Pt(d_{xz})$ and ≈44–46% first π(C≡C) fragment orbitals. The small variation in $\lambda_{calcd}=$ 413–435 nm is in agreement with the experimental results of λ_2 and is assigned to mixed $^1[d_\pi(Pt){\rightarrow}\pi^*(H_3tpy)]/^1[\pi(C{\equiv}C){\rightarrow}\pi^*(H_3tpy)]$ transitions.

Effect of acid on the electronic transitions of $[Pt(H_3tpy)\{C{\equiv}C(C_6H_4C{\equiv}C)_{n-1}C_6H_4\text{-}N(CH_3)_2\text{-}4\}]^+$ (n=1–3): TD-DFT results for the protonated forms of $[Pt(H_3tpy)\{C{\equiv}C(C_6H_4C{\equiv}C)_{n-1}C_6H_4\text{-}N(CH_3)_2\text{-}4\}]^+$ ($n=1$–3) are given in the Supporting Information (Table S6). Upon protonation of **12H**, **16H**, and **19H**, the calculated lowest singlet transition energies are: $\lambda_{calcd}=444$ (**12H**+H^+), 514 (**16H**+H^+) and 546 nm (**19H**+H^+), respectively, with the complexes in "cop" conformation, and are derived from HOMO→LUMO transitions and are described as $^1[\pi(C{\equiv}CAr){\rightarrow}\pi^*(H_3tpy)]$ transitions. For **12H**+H^+ ($n=1$), **16H**+H^+ ($n=2$), and **19H**+H^+ ($n=3$), the LUMOs are essentially H_3tpy-based; however, their HOMOs are mainly composed of the antibonding combinations of $Pt(d_{xz})$, π(C≡C), and Ar fragment orbitals, similar to the HOMOs of the $[Pt(H_3tpy)\{C{\equiv}C(C_6H_4C{\equiv}C)_{n-1}Ph\}]^+$ ($n=1$–3) series. As the number of nodes in the aryl–acetylide ligand increases with chain length n, the

HOMO energy increases, leading to a redshift in the HOMO→LUMO transition energy. With "per" conformations, the calculated allowed transitions are at $\lambda_{calcd}=398$, 412, and 418 nm for **12H**+H^+, **16H**+H^+, and **19H**+H^+, respectively. These absorption bands are less sensitive to chain length effects and are derived from HOMO−1 (or HOMO−2 for $n=3$)→LUMO transitions. The HOMO−1 (HOMO−2 at $n=3$) surfaces of **12H**+H^+, **16H**+H^+, and **19H**+H^+ are similar in character to the HOMO−n orbitals of **12H**, **16H**, and **19H** before protonation. This band is thus assigned as mixed $^1[d_\pi(Pt)\rightarrow\pi^*(H_3tpy)]/^1[\pi(C\equiv C)\rightarrow\pi^*(H_3tpy)]$ transitions.

*Energy gap ($\Delta E(S_0$–$T_1)$) of [Pt(H_3tpy)(C≡C−n*Pr*)]$^+$ and [Pt(H_3tpy){C≡C(C_6H_4C≡C)$_{n-1}$$C_6H_4$-X-4}]$^+$ (n=1–3, X=H, N(CH_3)$_2$ or N(CH_3)$_2$H$^+$)*: To gain insight into the effect of acids on the emission properties of the [Pt(tBu$_3$tpy){C≡C-(C_6H_4C≡C)$_{n-1}$$C_6H_4$-N($CH_3$)$_2$-4}] $^+$ ($n=1$–3) complexes, geometry optimizations were also carried out for the lowest triplet excited states (T_1) of both the nonprotonated and protonated forms. Geometry optimizations of [Pt(H_3tpy)-(C≡CR)]$^+$ (R=*n*Pr (**1H**)) and [Pt(H_3tpy){C≡C(C_6H_4-C≡C)$_{n-1}$$C_6H_4$-X-4}]$^+$ ($n=1$: (**7aH**), $n=2$: (**15H**), $n=3$: (**18H**) were also carried out at their lowest triplet excited states (T_1) for comparisons. Table 4 presents the energy gap

Table 4. PBE1PBE $\Delta E(S_0$–$T_1)$ energy gap [eV] for the model complexes [Pt(H_3tpy)(C≡C*n*Pr)]$^+$ (**1H**); [Pt(H_3tpy){C≡C(C_6H_4C≡C)$_{n-1}$Ph}]$^+$ ($n=1$ (**7aH**), $n=2$ (**15H**), and $n=3$ (**18H**)); and [Pt(H_3tpy){C≡C(C_6H_4-C≡C)$_{n-1}$$C_6H_4$-N($CH_3$)$_2$-4}/+H]$^{+/2+}$ ($n=1$ (**12H**), $n=2$ (**16H**), and $n=3$ (**19H**)) in CH_2Cl_2 before and after protonation modeled by PCM.

Complex	$\Delta E(S_0$–$T_1)$ [eV]	Complex	$\Delta E(S_0$–$T_1)$ [eV]
1H	2.59	**16H**	1.46
7aH	1.99	**16H**+H^+	2.01
12H	1.34	**18H**	1.81
12H+H^+	2.34	**19H**	1.56
15H	1.84	**19H**+H^+	1.89

$\Delta E(S_0$–$T_1)$ between the S_0 and T_1 states at their respective optimized geometries in CH_2Cl_2. It was found that $\Delta E(S_0$–$T_1)$ of [Pt(H_3tpy){C≡C(C_6H_4C≡C)$_{n-1}$-C_6H_4-X-4}]$^+$ ($n=1$–3) has a different chain length dependence between the X=H and N(CH_3)$_2$ series: the energy gap of the former decreases as n increases, while that of the latter increases as n increases. Protonation at the N(CH_3)$_2$ substituent of **12H**, **16H**, and **19H** leads to an increase in the energy gap $\Delta E(S_0$−$T_1)$.

Discussion

UV/Vis absorption spectroscopy: In general, the UV/Vis absorption spectra of [Pt(Y_3tpy)(C≡CR)]$^+$ (Y=*t*Bu or Cl, R=aryl; **5**–**22**) have two overlapping broad absorption bands with peak maxima at $\lambda_1=412$–640 nm and at $\lambda_2=383$–421 nm. Upon varying 1) the *para*-substituent of the aryl group and substituent of tpy ligand; 2) the chain length n with R=(C_6H_4C≡C)$_{n-1}$$C_6H_4$-X-4 ($n=1$–3: X=H or N-($CH_3$)$_2$; $n=1$–2: X=NH_2); 3) acidity of the medium with R=(C_6H_4C≡C)$_{n-1}$$C_6H_4$-X-4 ($n=1$–3: X=N($CH_3$)$_2$; $n=1$–2: X=NH_2); and 4) the solvent polarity, λ_2 spans a narrow spectral region (2360 cm^{-1}), and λ_1 changes over a wide spectral region (span of 8650 cm^{-1}). Based on the TDDFT results on model complexes [Pt(H_3tpy)(C≡CR)]$^+$ (R=aryl), these two absorption bands λ_1 and λ_2 are derived from two different electronic transitions. The lower energy absorption band λ_1 of [Pt(Y_3tpy)(C≡CR)]$^+$ (Y=*t*Bu or Cl, R=aryl) with the "cop" conformation is predominantly $^1[\pi(C\equiv C\text{-}Ar)\rightarrow\pi^*(Y_3tpy)]$ in character. The higher energy absorption band λ_2 of [Pt(Y_3tpy)(C≡CR)]$^+$ (Y=*t*Bu or Cl, R=aryl) with the "per" conformation is assigned to mixed $^1[d_\pi(Pt)\rightarrow\pi^*(Y_3tpy)]/^1[\pi(C\equiv C)\rightarrow\pi^*(Y_3tpy)]$ transitions.

*Substituent Effect of [Pt(Y_3tpy)(C≡CR)]$^+$ (Y=t*Bu or Cl, R=alkyl or aryl)*: The lowest energy absorption band, λ_1, is derived from a HOMO→LUMO transition of the complexes with the "cop" conformation as revealed from the TDDFT calculations. Since the HOMO energy of [Pt(tBu$_3$tpy)-(C≡CC_6H_4-X-4)]$^+$ increases with increasing electron-donating ability of the *para*-substituent X, λ_1 of [Pt(tBu$_3$tpy)-(C≡CC_6H_4-X-4)]$^+$ shows a concordant redshift and the λ_1 values are in the order of: **8** (21690 cm^{-1}; F)≈**10** (21690 cm^{-1}; Br)>**9** (21650 cm^{-1}; Cl)>**7a** (21550 cm^{-1}; H)>**14** (21010 cm^{-1}; Ph)>**11** (20410 cm^{-1}; OCH_3)>**13** (19230 cm^{-1}; NH_2)>**12** (17640 cm^{-1}; N(CH_3)$_2$).

A slight redshift of λ_1 is observed from **14** (476 nm; X=Ph) to **7a** (464 nm; X=H), and this could be due to lack of π-conjugation between the two adjacent phenyl rings of **14**. With R=9,9'-di-*n*-butyl-9H-fluorene (DBF; **20a**), the two phenyl rings are constrained to a coplanar geometry, leading to enhanced π-conjugation. Consequently, the λ_1 of **20a** (496 nm) shows a redshift from that of **14** (476 nm) by 850 cm^{-1}. Due to the π-conjugation and mesomeric effect of the amine groups,[2(a)] λ_1 of **22** (532 nm; R=(DBF)-NH_2) and **21a** (557 nm; R=(DBF)-N(CH_3)$_2$) show further redshifts from that of **20a**.

Similar to previous work on cyclometalated Pt^{II} complexes containing acetylide ligands,[17] modification of the terpyridine ligand with electron-withdrawing groups also leads to a redshift in the lowest absorption energy band. The LUMOs of [Pt(Y_3tpy)(C≡CR)]$^+$ complexes are tpy-based. Replacement of the tpy substituents Y from electron-donating *t*Bu to electron-withdrawing Cl group lowers the LUMO energy and, hence, the transition energy of [Pt-(Cl_3tpy)(C≡CR)]$^+$ decreases (λ_1 increases) from its *t*Bu counterpart as follows: **2a** (23310 cm^{-1}; Y=*t*Bu, X=*t*Bu)> **2b** (20700 cm^{-1}, Y=Cl, X=*t*Bu); **20a** (20160 cm^{-1}, Y=*t*Bu, X=-(DBDF)-H)>**20b** (18210 cm^{-1}, Y=Cl, X=-(DBDF)-H) and **21a** (17950 cm^{-1}, Y=*t*Bu, X=-(DBDF)-N(CH_3)$_2$)> **21b** (15630 cm^{-1}, Y=Cl, X=-(DBDF)-N(CH_3)$_2$) in CH_2Cl_2 and **7a** (23810 cm^{-1}; Y=*t*Bu, X=Ph)>**7b** (21010 nm, Y=Cl, X=Ph) in CH_3CN.

[Pt(tBu$_3$tpy){C≡C(C$_6$H$_4$C≡C)$_{n-1}$C$_6$H$_4$-X-4}]$^+$ (n=1–3: X=H or N(CH$_3$)$_2$; n=1–2, X=NH$_2$) with different chain lengths: For the aryl–acetylide complexes, **7a**, **15**, and **18** (X=H series), λ_1 shows a redshift with increase in chain length *n*, but for the amine-substituted aryl–acetylide complexes, **12**, **16**, and **19** (X=N(CH$_3$)$_2$ series) and **13** and **16** (X=NH$_2$ series), λ_1 shows a blueshift with increase in chain length *n*. The different chain length effect on the spectroscopic behavior of the X=H and N(CH$_3$)$_2$ series could be rationalized by the intrinsic difference in the nature of the HOMO participating in the ^{1}[π(C≡CAr)→π*(*t*Bu$_3$tpy)] transition. In the X=H series, the HOMO is fully delocalized over the entire aryl–acetylide ligand. A redshift trend is observed in [Pt(*t*Bu$_3$tpy){C≡C(C$_6$H$_4$C≡C)$_{n-1}$C$_6$H$_4$-X-4}]$^+$ (X=H, *n*=1 (**7a**), *n*=2 (**15**) and *n*=3 (**18**)) and is explained by a greater conjugation across the [-C≡C(C$_6$H$_4$C≡C)$_{n-1}$Ph] chains with increasing *n* values.[6,7,9,37] However, in the X=N(CH$_3$)$_2$ series, the HOMO is essentially localized on the C$_6$H$_4$-N(CH$_3$)$_2$-4 unit. As the separation between donor orbital (HOMO) and acceptor orbital (LUMO) increases as *n* increases, the electrostatic attraction between these orbitals decreases, and thus λ_1 of [Pt(*t*Bu$_3$tpy){C≡C(C$_6$H$_4$C≡C)$_{n-1}$C$_6$H$_4$-N(CH$_3$)$_2$-4}]$^+$ show blueshifts with an increase in chain length *n*.

Effect of acid on the electronic transitions of [Pt(tBu$_3$tpy){C≡C(C$_6$H$_4$C≡C)$_{n-1}$C$_6$H$_4$-N(CH$_3$)$_2$-4}]$^+$ (n=1–3): Upon addition of acid to the amine-bearing aryl–acetylide complexes (**12**, **13**, **16**, **17**, and **19**), λ_1 shows a blueshift with magnitude in the order of: **12** (*n*=1, 6640 cm^{-1})>**16** (*n*=2, 1960 cm^{-1})>**19** (*n*=3, ≈0 cm^{-1}); and **13** (*n*=1, 5520 cm^{-1})>**17** (*n*=2, 1720 cm^{-1}). This observation could be explained by the DFT results that the HOMOs of **12H**, **16H**, and **19H** are localized on the C$_6$H$_4$-N(CH$_3$)$_2$-4 unit before protonation. Addition of H$^+$ on the N atom of the amine substituent on the aryl–acetylide ligands of **12H**, **16H**, and **19H** leads to a change in the nature of the HOMOs from being localized on the C$_6$H$_4$-N(CH$_3$)$_2$-4 unit to being delocalized over the entire aryl–acetylide ligands, similar to the HOMOs of the nonsubstituted [Pt(*t*Bu$_3$tpy){C≡C(C$_6$H$_4$C≡C)$_{n-1}$Ph}]$^+$ series (*n*=1, **7a**; *n*=2, **15**; *n*=3, **18**). Consequently, the λ_1 value of the protonated forms of **12**, **16**, and **19** show redshifts with increasing chain length *n* from 1 to 3 (λ_1=412 nm for *n*=1, 448 nm for *n*=2, and 480 nm for *n*=3 with X=N(CH$_3$)$_2$ and λ_1=409 nm for *n*=1, 446 nm for *n*=2 with X=NH$_2$).

It should be noted that, from the TDDFT results of the protonated forms of **12H**, **16H**, and **19H**, the calculated lowest absorption energies correspond to their respective HOMO → LUMO transitions with λ_{calcd}=444, 514, and 546 nm for **12H**+H$^+$, **16H**+H$^+$, and **19H**+H$^+$, respectively. These transition energies all show blueshifts from the calculated lowest absorption energies of the corresponding nonprotonated forms (λ_{calcd}=732, 714, and 683 nm for **12H**, **16H**, and **19H**, respectively), in disagreement with the experimental results that the lowest energy absorption band of **19** is essentially unshifted after addition of acid. However, when compared to the second lowest absorption energies calculated ($\lambda_{calcd,2}$=598, 566, and 543 nm for **12H**, **16H**, and **19H**, respectively), the calculated magnitude of blueshifts are in good agreement with the experimental findings.

Insight from electronic and resonance Raman spectroscopy: Resonance Raman (RR) spectroscopy is informative in probing the structural distortion upon electronic excitation. Excitation of **11** at 416 and 502.9 nm gave distinctly different results, in which the ν(C≡C) stretch mode at 2100 cm^{-1} is doubly enhanced in the latter excitation. This implies that the electronic transition at 502.9 nm involves a larger structural distortion of the C≡C unit than at 416 nm. It is noted that the ν(C=C) and ν(C=N) stretching mode, at 1300–1600 cm^{-1} are observed at both 416 and 502.9 nm excitations, and these stretching modes originate from the aryl groups of acetylide and terpyridine ligands. The RR findings are supportive to the assignment of [Pt(Y$_3$tpy)(C≡CR)]$^+$ (Y=*t*Bu or Cl, R=aryl) that the lower energy band (λ_1) comes from ^{1}LLCT ^{1}[π(C≡CAr)→π*(tpy)] transitions, whereas the high-energy band (416 nm) is derived from ^{1}MLCT/^{1}LLCT of ^{1}[d$_\pi$(Pt)→π*(tpy)]/^{1}[π(C≡C)→π*(tpy)] transitions.

Emission spectroscopy: Based on the DFT calculations on model complexes [Pt(H$_3$tpy)(C≡CR)]$^+$ (R=*n*Pr (**1H**), Py (**6H**), Ph (**7aH**), and C$_6$H$_4$-N(CH$_3$)$_2$-4 (**12H**)), [Pt(H$_3$tpy){C≡C(C$_6$H$_4$C≡C)$_{n-1}$Ph}]$^+$ (*n*=1 (**7aH**), *n*=2 (**15H**) and *n*=3 (**18H**)), [Pt(H$_3$tpy){C≡C(C$_6$H$_4$C≡C)$_{n-1}$C$_6$H$_4$-N(CH$_3$)$_2$-4}]$^+$ (*n*=1 (**12H**), *n*=2 (**16H**) and *n*=3 (**19H**)), their SOMOs (singly occupied molecular orbital) and SOMOs−1 at the optimized lowest triplet excited state (T$_1$) have similar parentages as the LUMOs and HOMOs at the optimized singlet ground state (S$_0$), respectively. These model complexes at the optimized T$_1$ geometries have the same frontier molecular orbital (FMO) orderings as their corresponding singlet ground states (S$_0$). Hence, discussion on the emission properties of [Pt(Y$_3$tpy)(C≡CR)]$^+$ (Y=*t*Bu or Cl, R=alkyl or aryl) **1**–**22** is based on the assignments of their low-energy absorption bands (see above).

Substituent and chain length effects of [Pt(Y$_3$tpy)(C≡CR)]$^+$ (Y=tBu or Cl, R=alkyl or aryl): Since the lowest energy electronic transitions of [Pt(Y$_3$tpy)(C≡CR)]$^+$ (Y=*t*Bu or Cl, R=alkyl) originate from mixed ^{1}[d$_\pi$(Pt)→π*(Y$_3$tpy)]/^{1}[π(C≡C)→π*(Y$_3$tpy)] transitions, the emissions of the alkyl–acetylide complexes **1**, **2a**, **3**, and **4** at λ_{max}=547–548 nm in CH$_2$Cl$_2$ at 298 K and at ≈498–499 nm in glassy *n*BuCN at 77 K, are derived from excited states with mixed ^{3}[d$_\pi$(Pt)→π*(tpy)]/^{3}[π(C≡C)→π*(tpy)] character. From TDDFT calculations, the mixed ^{1}[d$_\pi$(Pt)→π*(H$_3$tpy)]/^{1}[π(C≡C)→π*(H$_3$tpy)] transition of [Pt(H$_3$tpy)(C≡CR)]$^+$ of **1H** (R=alkyl) occurs at a lower energy than those of **6H**, **7aH**, **12H**, **15H**, **16H**, **18H**, and **19H** (R=aryl). For example, TDDFT calculations gave λ_{calcd}=451 nm for **1H** (R=*n*Pr) and λ_{calcd}=409 nm for **7aH** (R=Ph) and these λ_{calcd} are assigned as deriving from mixed ^{1}[d$_\pi$(Pt)→π*(H$_3$tpy)]/^{1}[π(C≡C)→π*(H$_3$tpy)] transitions. Correspondingly, the mixed ^{3}[d$_\pi$(Pt)→

$\pi^*(tpy)]/^3[\pi(C\equiv C)\rightarrow\pi^*(tpy)]$ excited states of $[Pt(H_3tpy)(C\equiv CR)]^+$ (R = aryl; **6H**, **7aH**, **12H**, **15H**, **16H**, **18H**, and **19H**) are also expected to be at higher energies than that of **2H** (R = alkyl). However, the $[Pt(tBu_3tpy)(C\equiv CR)]^+$ (R = aryl) complexes emit at a lower energy than those with R = alkyl (see Table 1). This could be explained by assigning the emission of $[Pt(Y_3tpy)(C\equiv CR)]^+$ (Y = *t*Bu or Cl; R = aryl) as being derived from $^3[\pi(C\equiv CAr)\rightarrow\pi^*(Y_3tpy)]$ instead of the mixed $^3[d_\pi(Pt)\rightarrow\pi^*(tpy)]/^3[\pi(C\equiv C)\rightarrow\pi^*(tpy)]$ excited states.

Two factors affect the ^{3}LLCT transition energies of $[Pt(Y_3tpy)(C\equiv CR)]^+$ (Y = *t*Bu or Cl; R = aryl). One is the SOMO−1 energy which is increased by the electron-donating ability, π-conjugation, and chain length *n* of the aryl–acetylide ligand. The other is the SOMO energies which are decreased by changing the Y substituents from electron-donating *t*Bu to electron-withdrawing Cl. These two factors lead to the following findings: 1) there is a moderate redshift in emission energy of $[Pt(tBu_3tpy)(C\equiv CC_6H_4\text{-}X\text{-}4)]^+$ upon increase in the electron-donating ability of the *para*-substituent X; 2) the emission energy decreases from 18830 cm^{-1} for **14** ($R = C_6H_4$-Ph-4) to 18210 cm^{-1} for **20a** (R = -(DBF)) in glassy *n*BuCN at 77 K due to extended π-conjugation in the latter; 3) the emission energy of $[Pt(tBu_3tpy)\{C\equiv C(C_6H_4C\equiv C)_{n-1}Ph\}]^+$ shows a redshift with increase in chain length *n* from 1 to 3; and 4) the emission energy of $[Pt(Y_3tpy)(C\equiv CR)]^+$ shows a redshift upon replacing Y from *t*Bu to Cl. **2a** (Y = *t*Bu ; R = *t*Bu, 20080 cm^{-1}) and **2b** (Y = Cl ; R = *t*Bu,18980 cm^{-1}); **20a** (Y = *t*Bu; R = -(DBF), 18210 cm^{-1}) and **20b** (Y = Cl; R = -(DBF), 16470 cm^{-1}) in glassy *n*BuCN at 77 K.

Effect of acid on the electronic transitions of $[Pt(tBu_3tpy)\{C\equiv C(C_6H_4C\equiv C)_{n-1}C_6H_4\text{-}X\text{-}4\}]^+$ (n=1–3, X=N(CH$_3$)$_2$; n = 1–2, X=NH$_2$): Similar to the reports on related amine-containing aryl–acetylide–platinum(II) complexes,[1a,b,2a,4,14] complexes **12** (*n* = 1, X = N(CH$_3$)$_2$), **13** (*n* = 1, X = NH$_2$), and **17** (*n* = 2, X = NH$_2$) are nonemissive in neutral CH_2Cl_2 solutions, but become emissive in the presence of acids. To support these findings, the energy gap ($\Delta E(S_0\text{-}T_1)$) at the respective gas-phase-optimized geometries of the S_0 and T_1 states were calculated. The energy gap law states that the nonradiative decay rate k_{nr} decreases exponentially with the energy gap $\Delta E(S_0\text{–}T_1)$,[16] so that a small $\Delta E(S_0\text{–}T_1)$ could result in a lack of emission. $\Delta E(S_0\text{–}T_1)$ of **7a** is 1.99 eV, and its emission is derived from the $^3[\pi(C\equiv CAr)\rightarrow\pi^*(tBu_3tpy)]$ excited state. Compared to **7aH**, **12H** has a smaller $\Delta E(S_0\text{–}T_1)$ (1.34 eV). It is, therefore, likely that the lack of emission of **12** is due to the small $\Delta E(S_0\text{–}T_1)$. Upon protonation of **12H** at the amine substituent, $\Delta E(S_0\text{–}T_1)$ increases dramatically to 2.34 eV, which is even higher in energy than that of **7aH** (1.99 eV). Since the emissive state of **7aH** is $^3[\pi(C\equiv CAr)\rightarrow\pi^*(tBu_3tpy)]$ in nature, the much larger $\Delta E(S_0\text{–}T_1)$ of the protonated form of **12H** should also create an emissive $^3[\pi(C\equiv CAr)\rightarrow\pi^*(tpy)]$ excited state based solely on the energy gap law. It is thus proposed that the emission of the protonated forms of $[Pt(tBu_3tpy)\{C\equiv C(C_6H_4C\equiv C)_{n-1}C_6H_4\text{-}X\text{-}4\}]^+$ (X = N(CH$_3$)$_2$ for **12** (*n* = 1), **16** (*n* = 2), **19** (*n* = 3), or NH$_2$ for **13** (*n* = 1) and **17** (*n* = 2) are derived from the $^3[\pi(C\equiv CAr)\rightarrow\pi^*(tBu_3tpy)]$ instead of the $^3[d_\pi(Pt)\rightarrow\pi^*(tpy)]/^3[\pi(C\equiv C)\rightarrow\pi^*(tpy)]$ excited state, although the latter is usually proposed in the literature to be the emissive excited state. Complexes **16** and **19** are emissive both in the presence and absence of acids. This is probably due to the fact that as the chain length *n* of the aryl–acetylide ligand increases, the calculated energy gap $\Delta E(S_0\text{–}T_1)$ also increases from 1.34 (**12H**, *n* = 1) to 1.46 (**16H**, *n* = 2), and to 1.56 eV (**19H**, *n* = 3). As a result, the nonradiative decay rates of **16** and **19** become smaller, and, thus, these two complexes are emissive even in the absence of acids.

Conclusion

In this work, a combination of spectroscopic and computational approaches were employed to investigate the photophysical properties of square-planar platinum(II) complexes bearing terpyridine and acetylide ligands, $[Pt(Y_3tpy)(C\equiv CR)]^+$. It has been reported that rotation about the metal–carbon bond in metal–acetylide complexes[18] is essentially frictionless at ambient temperature due to the cylindrical symmetry of the triple bond, which is able to maintain conjugation between the metal and the aromatic plane irrespective of their relative orientations. Thus, it can adopt conformations coplanar ("cop") or perpendicular ("per") to the terpyridine ligand in $[Pt(Y_3tpy)(C\equiv CR)]^+$. The lowest absorption energy, λ_1, is derived from the $^1[\pi(C\equiv CAr)\rightarrow\pi^*\text{-}(H_3tpy)]$ excited state with the "cop" conformation, whereas the second lowest absorption energy, λ_2, is from mixed $^1[d_\pi(Pt)\rightarrow\pi^*(tpy)]/^1[\pi(C\equiv C)\rightarrow\pi^*(tpy)]$ excited states with the "per" conformation. Such an assignment is also in accordance with the significant solvatochromic effects of λ_1 and only a slight blueshift in λ_2 upon increase in solvent polarity. The emissions of the alkyl–acetylide complexes of $[Pt(Y_3tpy)(C\equiv CR)]^+$ are due to mixed $^3[d_\pi(Pt)\rightarrow\pi^*(tpy)]/^3[\pi\text{-}(C\equiv C)\rightarrow\pi^*(tpy)]$ excited states; however, the emissions of the aryl analogues were found to originate from the $^3[\pi\text{-}(C\equiv CAr)\rightarrow\pi^*(H_3tpy)]$ excited states.

It was demonstrated that the photophysical properties of $[Pt(tBu_3tpy)\{C\equiv C(C_6H_4C\equiv C)_{n-1}C_6H_4\text{-}X\text{-}4\}]^+$ complexes show different chain length *n* dependence: when X = H, λ_1 shows a redshift with *n*, but, when X = N(CH$_3$)$_2$, λ_1 shows a blueshift with *n*. This is due to the different nature of the HOMO of these two series of complexes. For the X = H series, the HOMO is fully delocalized over the entire aryl–acetylide ligand, but, for the X = N(CH$_3$)$_2$ series, the HOMO is localized on the C_6H_4-N(CH$_3$)$_2$-4 moiety. Upon addition of acid, the amine substituent no longer contributes to the HOMO, and the HOMO of the protonated form of the X = N(CH$_3$)$_2$ series become delocalized over the entire aryl–acetylide ligand, similar to those of the X = H series, and hence the amine series also has a redshift in λ_1 with increasing chain length *n* after addition of acid.

As reported in the literature, $[Pt(tBu_3tpy)(C\equiv C\text{-}C_6H_4\text{-}X\text{-}4)]^+$ bearing amine substituents (X = NH$_2$ and N(CH$_3$)$_2$) are

nonemissive at room temperature in CH_2Cl_2. However, [Pt(tBu$_3$tpy){C≡C(C$_6$H$_4$C≡C)$_{n-1}$C$_6$H$_4$-N(CH$_3$)$_2$-4}]$^+$ are weakly emissive under similar conditions and all of the amine-bearing aryl–acetylide complexes become emissive at 298 K upon addition of acid. This photophysical behavior could be explained by invoking the energy gap law, in which the energy gap between the singlet ground state and the first triplet excited state is the smallest when $n=1$ and this gap increases with increase in chain length n and upon addition of acid.

Experimental Section

General: [Pt(tBu$_3$tpy)Cl]ClO$_4$[10] and acetylenes[11] were prepared according to literature methods. (Caution: perchlorate salts are potentially explosive and should be handled with care and in small amounts.) [Pt(Cl$_3$tpy)Cl]OTf was synthesized by modification of a literature method.[9] The solvents used for synthesis were of analytical grade and purified according to conventional methods.[29] All solvents for photophysical studies were of HPLC grade. Fast atom bombardment (FAB) mass spectra were obtained on a Finnigan Mat 95 mass spectrometer with a 3-nitrobenzyl alcohol matrix. ^{1}H (500 MHz), ^{13}C (126 MHz) and ^{19}F (376 MHz) NMR measurements were performed on a Bruker DPX 500 FT-NMR spectrometer with tetramethylsilane (^{1}H and ^{13}C) and CF$_3$COOH (^{19}F) as references. Elemental analyses were performed by the Institute of Chemistry at the Chinese Academy of Sciences, Beijing. Infrared spectra were recorded on a Bio-Rad FT-IR spectrophotometer. UV/Vis spectra were recorded on a Perkin–Elmer Lambda 19 UV/Vis spectrophotometer or on a Hewlett–Packard 8453 spectrophotometer. The [Pt(Y$_3$tpy)(C≡CR)]$^+$ complexes were prepared following the cross-coupling reactions of [Pt(Y$_3$tpy)Cl]$^+$ with HC≡CR, details of which are given in the Supporting Information.

Emission and lifetime measurements: Steady-state excitation and emission spectra were recorded on a SPEX 1681 Fluorolog-2 Model F111AI spectrophotometer. Solution samples for measurements were degassed with at least four freeze-pump-thaw cycles. Low-temperature (77 K) emission spectra for glassy and solid-state samples were recorded in 5 mm diameter quartz tubes, which were placed in a liquid nitrogen Dewar equipped with quartz windows. The emission spectra were corrected for monochromator and photomultiplier efficiency and for xenon lamp stability. Emission lifetime measurements were performed with a Quanta Ray DCR-3 pulsed Nd:YAG laser system (pulse output 355 nm, 8 ns). The emission signals were detected by a Hamamatsu R928 photomultiplier tube and recorded on a Tektronix TDS 350 oscilloscope. Errors for λ values ($\pm$1 nm), τ ($\pm$10%), Φ ($\pm$10%) were estimated. The emission quantum yields were determined using the method of Demas and Crosby[28] with [Ru(bpy)$_3$]PF$_6$ in degassed CH$_3$CN as a standard reference solution ($\Phi_r=0.062$).

Computational details: The 18-valence electron Stuttgart small core relativistic pseudo-potentials with their corresponding optimized set of basis functions were employed for the Pt atom[19] with all other atoms using the standard split-valence 6–31G* basis set[20] for all calculations. The calculated wavelength value is labeled as λ_{calcd}. The *tert*-butyl groups on the Y$_3$tpy ligand are replaced by hydrogen atoms (H$_3$tpy) to save computational cost. The singlet ground (S_0) and the lowest triplet (T_1) excited states were partially optimized using the density functional theory (DFT) method with the aryl–acetylide ligand being constraint to be coplanar ("cop") and perpendicular to ("per") the tpy ligand. The low-lying S_0–S_n transition energies at the optimized singlet ground states were calculated using time-dependent density functional theory (TDDFT).[21] The electrostatic solvent effect was taken into account in the excitation energy calculations using the polarizable continuum model (PCM)[22] with the solvation energies evaluated by a cavity model, namely, the united atoms topological model.[23] The density functional PBE1PBE[24] was employed for both geometry optimizations and excited state calculations. This function has been shown to reproduce charge transfer bands in metal complexes in both the gas phase[25] and in solution.[26] All calculations were performed using the Gaussian 03 program package.[27] RR spectra were acquired by using the apparatus and methods previously detailed in references [8] and [30].

Acknowledgements

We thank the Research Grants Council of the Hong Kong SAR, China (HKU 7008/09); National Natural Science Foundation of China/Research Grants Council Joint Research Scheme (N HKU 752/08), the Chinese Academy of Sciences/Croucher Foundation Funding Scheme for Joint Laboratories and the University Development Fund for Synthetic Chemistry of the University of Hong Kong for financial support. We are grateful to the support from the AoEprogram for the Institute of Molecular Functional Materials (10208976).

[1] a) K. M.-C. Wong, V. W.-W. Yam, *Coord. Chem. Rev.* **2007**, *251*, 2477–2488, and references therein; b) K. M. C. Wong, W. S. Tang, X.-X. Lu, N. Zhu, V. W.-W. Yam, *Inorg. Chem.* **2005**, *44*, 1492–1498; c) P. Jarosz, K. Lotito, J. Schneider, D. Kumaresan, R. Schmehl, R. Eisenberg, *Inorg. Chem.* **2009**, *48*, 2420; d) P. Du, J. Schneider, P. Jarosz, J. Zhang, W. W. Brennessel, R. Eisenberg, *J. Phys. Chem. B* **2007**, *111*, 6887–6894; e) R. Narayana-Prabhu, R. H. Schmehl, *Inorg. Chem.* **2006**, *45*, 4319–4321; f) X.-J. Liu, J.-K. Feng, J. Meng, Q.-J. Pan, A.-M. Ren, X. Zhou, H.-X. Zhang, *Eur. J. Inorg. Chem.* **2005**, 1856–1866; g) X. Zhou, Q.-J. Pan, T. Liu, M.-X. Li, H. X. Zhang, *J. Mol. Struct.* **2008**, *871–892*, 91–98; h) C. Monnereau, J. Gomez, E. Blart, F. Odobel, S. Wallin, A. Fallberg, L. Hammarström, *Inorg. Chem.* **2005**, *44*, 4806–4817; i) A. Scarpaci, C. Monnereau, N. Hergué, E. Blart, S. Legoupy, F. Ododel, A. Gorfo, J. Pérez-Moreno, K. Clays, I. Asselberg, *Dalton Trans.* **2009**, 4538–4546; j) M.-X. Zhu, W. Lu, N. Zhu, C.-M. Che, *Chem. Eur. J.* **2008**, *14*, 9736–9746.

[2] a) F. Guo, W. Sun, Y. Liu, K. Schanze, *Inorg. Chem.* **2005**, *44*, 4055–4065; b) W. Sun, Z.-X. Wu, Q.-Z. Yang, L.-Z. Wu, C.-H. Tung, *Appl. Phys. Lett.* **2003**, *82*, 850–852.

[3] a) B. Ventura, A. Barbieri, A. Zanelli, F. Barigelletti, J. B. Seneclauze, S. Diring, R. Ziessel, *Inorg. Chem.* **2009**, *48*, 6409–6416; b) E. Shikhova, E. O. Danilov, S. Kinayyigit, I. E. Pomestchenko, A. D. Tregubov, F. Camerel, P. Retailleau, R. Ziessel, F. N. Castellano, *Inorg. Chem.* **2007**, *46*, 3038–3048; c) R. Ziessel, S. Diring, P. Retailleau, *Dalton Trans.* **2006**, 3285–3290.

[4] a) X. Han, L.-Z. Wu, G. Si, J. Pan, Q.-Z. Yang, L.-P. Zhang, C.-H. Tung, *Chem. Eur. J.* **2007**, *13*, 1231–1239; b) Q.-Z. Yang, Q.-X. Tong, L.-Z. Wu, Z.-X. Wu, L.-P. Zhang, C.-H. Tung, *Eur. J. Inorg. Chem.* **2004**, 1948.

[5] C.-Y. Wong, M. C.-W. Chan, N. Zhu, C.-M. Che, *Organometallics* **2004**, *23*, 2263–2272.

[6] H.-Y. Chao, W. Lu, Y. Li, M. C.-W. Chan, C.-M. Che, K. K. Cheung, N. Zhu, *J. Am. Chem. Soc.* **2002**, *124*, 14696–14706.

[7] a) T. M. Cooper, D. M. Krein, A. R. Burke, D. G. McLean, J. E. Rogers, J. E. Slagle, P. A. Fleitz, *J. Phys. Chem. A* **2006**, *110*, 4369–4375; b) J. E. Rogers, B. C. Hall, D. C. Hufnagle, J. E. Slagle, A. P. Ault, D. G. McLean, P. A. Fleitz, T. M. Cooper, *J. Chem. Phys.* **2005**, *122*, 214708–1–8.

[8] C.-Y. Wong, C.-M. Che, M. C. W. Chan, J. Han, K.-H. Leung, D. L. Phillips, K.-Y. Wong, N. Zhu, *J. Am. Chem. Soc.* **2005**, *127*, 13997–14007.

[9] S.-C. Chan, M. C. W. Chan, Y. Wang, C.-M. Che, K.-K. Cheung, N. Zhu, *Chem. Eur. J.* **2001**, *7*, 4180–4190.

[10] S.-W. Lai, M. C. W. Chan, K.-K. Cheung, C.-M. Che, *Inorg. Chem.* **1999**, *38*, 4262–4267.

[11] a) Y.-G. Zhi, S.-W. Lai, Q. K.-W. Chan, Y.-C. Law, G. S.-M. Tong, C.-M. Che, *Eur. J. Org. Chem.* **2006**, 3125–3139; b) C. J. Kelley, A. Ghiorghis, J. M. Kauffman, *J. Chem. Res.* **1997**, 446–447.
[12] S. H. Hobert, J. T. Carney, S. D. Cummings, *Inorg. Chim. Acta* **2001**, *318*, 89–96.
[13] CCDC-752736 (**2a**), 752737 (**4**), 752738 (**5**·2CH_3CN), 752739 (**6**·CH_3CN), 752740 (**7a**·2CH_3CN), 752741 (**9**·2CH_3CN), 752742 (**10**·2CH_3CN), and 752743 (**11**·2CH_3CN) contain the supplementary crystallographic data for this paper. These data can be obtained free of charge from The Cambridge Crystallographic Data Centre via www.ccdc.cam.ac.uk/data_request/cif.
[14] a) K. M.-C. Wong, W.-S. Tang, B. W.-K. Chu, N. Zhu, V. W.-W. Yam, *Organometallics* **2004**, *23*, 3459–3465; b) V. W.-W. Yam, R. P.-L. Tang, K. M.-C. Wong, K.-K. Cheung, *Organometallics* **2001**, *20*, 4476–4482.
[15] C. A. Hunter, J. K. M. Sanders, *J. Am. Chem. Soc.* **1990**, *112*, 5525–5534.
[16] R. Englman, J. Jortner, *Mol. Phys.* **1970**, *18*, 145–164.
[17] W. Lu, M. C. W. Chan, N. Zhu, C.-M. Che, C. Li, Z. Hui, *J. Am. Chem. Soc.* **2004**, *126*, 7639–7651.
[18] K. Costuas, F. Paul, L. Toupet, J.-F. Halet, C. Lapinte, *Organometallics* **2004**, *23*, 2053–2068.
[19] D. Andrae, U. Haeussermann, M. Dolg, H. Stoll, H. Preuss, *Theor. Chim. Acta* **1990**, *77*, 123–141.
[20] a) P. C. Hariharan, J. A. Pople, *Theor. Chim. Acta* **1973**, *28*, 213–222; b) M. M. Francl, W. J. Pietro, W. J. Hehre, J. S. Binkley, M. S. Gordon, D. J. DeFrees, J. A. Pople, *J. Chem. Phys.* **1982**, *77*, 3654–3665.
[21] a) M. E. Casida, *Recent Advances in Density Functional Methods, Part 1*, World Scientific, Singapore, **1995**; b) E. K. U. Gross, J. F. Dobson, M. Petersilka, *Density Functional Theory of Time-Dependent Phenomena*, Springer, Heidelberg, **1996**.
[22] J. Tomasi, M. Persico, *Chem. Rev.* **1994**, *94*, 2027–2094.
[23] V. Barone, M. Cossi, J. Tomasi, *J. Chem. Phys.* **1997**, *107*, 3210–3221.
[24] a) C. Adamo, V. Barone, *J. Chem. Phys.* **1999**, *110*, 6158–6170; b) J. P. Perdew, K. Burke, M. Ernzerhof, *Phys. Rev. Lett.* **1996**, *77*, 3865–3868.
[25] C. Adamo, V. Barone, *Theor. Chem. Acc.* **2000**, *105*, 169–172.
[26] a) V. Barone, F. F. de Biani, E. Ruiz, B. Sieklucka, *J. Am. Chem. Soc.* **2001**, *123*, 10742–10743; b) J.-F. Guillemoles, V. Barone, L. Joubert, C. Adamo, *J. Phys. Chem. A* **2002**, *106*, 11354–11360.
[27] Gaussian 03, Revision B.05, M. J. Frisch, G. W. Trucks, H. B. Schlegel, G. E. Scuseria, M. A. Robb, J. R. Cheeseman, J. A. Montgomery, Jr., T. Vreven, K. N. Kudin, J. C. Burant, J. M. Millam, S. S. Iyengar, J. Tomasi, V. Barone, B. Mennucci, M. Cossi, G. Scalmani, N. Rega, G. A. Petersson, H. Nakatsuji, M. Hada, M. Ehara, K. Toyota, R. Fukuda, J. Hasegawa, M. Ishida, T. Nakajima, Y. Honda, O. Kitao, H. Nakai, M. Klene, X. Li, J. E. Knox, H. P. Hratchian, J. B. Cross, V. Bakken, C. Adamo, J. Jaramillo, R. Gomperts, R. E. Stratmann, O. Yazyev, A. J. Austin, R. Cammi, C. Pomelli, J. W. Ochterski, P. Y. Ayala, K. Morokuma, G. A. Voth, P. Salvador, J. J. Dannenberg, V. G. Zakrzewski, S. Dapprich, A. D. Daniels, M. C. Strain, O. Farkas, D. K. Malick, A. D. Rabuck, K. Raghavachari, J. B. Foresman, J. V. Ortiz, Q. Cui, A. G. Baboul, S. Clifford, J. Cioslowski, B. B. Stefanov, G. Liu, A. Liashenko, P. Piskorz, I. Komaromi, R. L. Martin, D. J. Fox, T. Keith, M. A. Al-Laham, C. Y. Peng, A. Nanayakkara, M. Challacombe, P. M. W. Gill, B. Johnson, W. Chen, M. W. Wong, C. Gonzalez, J. A. Pople, Gaussian, Inc., Wallingford CT, **2004**.
[28] J. N. Demas, G. A. Crosby, *J. Phys. Chem.* **1971**, *75*, 991–1024.
[29] D. D. Perrin, W. L. F. Armarego, D. R. Perrin, *Purification of Laboratory Chemicals*, 2nd ed., Pergamon, Oxford, **1980**.
[30] a) K. H. Leung, D. L. Phillips, M. C. Tse, C. M. Che, V. M. Miskowski, *J. Am. Chem. Soc.* **1999**, *121*, 4799–4803; b) C. M. Che, M. C. Tse, M. C. W. Chan, K. K. Cheung, D. L. Phillips, K. H. Leung, *J. Am. Chem. Soc.* **2000**, *122*, 2464–2468.

Received: November 5, 2009
Published online: April 26, 2010

